Bindi, D., Petrovic, B., Karapetrou, S., Manakou, M., Boxberger, T., Raptakis, D., Pitilakis, K. D., Parolai, S. (2015): Seismic response of an 8-story RC-building from ambient vibration analysis. - *Bulletin of Earthquake Engineering*, *13*, 7, p. 2095-2120.

DOI: http://doi.org/10.1007/s10518-014-9713-y

Seismic response of an 8-story RC-building from ambient vibration analysis

D. Bindi, B. Petrovic, S. Karapetrou, M. Manakou, T. Boxberger, D. Raptakis, K.D. Pitilakis S. Parolai

Abstract

In this study, we assess the dynamic characteristics of a 8-story RC-building composed by two units connected through a structural joint. This building, belonging to one of the largest hospitals in northern Greece, has been selected in the framework of an European funded project (REAKT) as test site for developing a Structural Health Monitoring system and it is instrumented with a permanent strong motion network. The assessment of the dynamic characteristics is performed using ambient vibration recorded by a temporary seismic network installed inside the structure. Non-parametric identification methods, namely the Peak Picking and Frequency Domain decomposition, are applied to perform operational modal analysis and extract the natural frequencies and mode shapes of the structural system. Since the detection of changes in the shear wave velocity inside the building is relevant for Health Monitoring analysis, we use the ambient vibration recordings to perform a deconvolution interferometry. Moreover, a shear-beam model is considered to estimate the velocity in the first three floors, where the distribution of internal sources introduces complex patterns in the impulse response functions. The velocity for lowest part of the building is estimated by optimizing the match between the arrival times of the empirical and theoretical pulses. Finally, the velocities and quality factors estimated from ambient vibration analysis are consistent with preliminary results obtained analyzing earthquake data recorded in the same building.

1 Introduction

The rapid development of data acquisition and processing capabilities has given rise to major advances in the experimental operational studies, particularly in the field of structural health monitoring. Monitoring of civil structures is becoming increasingly popular as it offers the opportunity to better understand the dynamic behavior of structures under seismic loading, measuring the structural response and monitoring the damage evolution. Therefore it is considered a significant tool for seismic protection and risk mitigation ensuring the integrity and improving the performance and reliability of structures.

The seismic response of a building can be determined looking either at the characteristics of the normal modes (vibrational approach, e.g. Chopra, 1996) or at the properties of seismic waves propagating within the building (waveform approach, e.g., Kanai, 1965; Todorovska and Trifunac, 1990; Snieder and Şafak, 2006; Todorovska, 2009; Rahmani and Todorovska, 2013; Nakata et al., 2013). Dynamic characterization of civil engineering structures (frequencies, mode shapes, damping ratios) is of major importance in a wide range of research and application fields, such as dynamic response prediction, finite element model updating, structural health monitoring and vibration control engineering. Since a limited number of moderate to strong earthquakes occur per year close to well instrumented buildings, which are anyway few, the dynamic characteristics of civil engineering structures are generally extracted from the building response to forced vibrations, weak/moderate earthquakes and ambient vibrations, limited however to the range of linear deformation. Although the origin of using ambient vibration for building monitoring started long time ago (e.g. Davinson, 1924; Carder, 1936; Housner and Brady, 1963; Trifunac, 1972; Ivanović et al, 2000), the development of several system identification techniques in the context of modal analysis of output only systems, made this kind of monitoring approach very popular in the last two decades (e.g. Brincker et al., 2001; Van Overschee and De Moor, 1996; Peeters and De Roeck, 1999). Operational Modal Analysis (OMA) is generally preferred to forced vibration measurements due to the fact that the same modal parameters can be obtained from vibration data in operational rather than laboratory conditions (Reynders, 2012). There are several studies that have used ambient vibration testing for the identification of the dynamic behavior of civil engineering structures (Brownjohn, 2003; Ventura et al., 2003), finite element calibration and updating (Teughels, 2003; Jaishi and Ren, 2005), vulnerability assessment (Guéguen et al., 2007; Michel et al., 2008; Michel et al., 2012) and damage detection (Peeters, 2000).

In the context of the waveform approach, the application of ambient vibration has been pushed by the introduction of the deconvolution interferometry (e.g. Snieder and Şafak, 2006). Seismic interferometry (Aki, 1957; Clearbout, 1968; Snieder and Şafak, 2006) is based on the correlation of waves recorded at different receivers; under some assumptions on the source distribution, it can be used to retrieve the Green's function that accounts for the wave propagation between the two receivers (e.g. Lobkis and Weaver, 2001; Wapenaar, 2004). This technique has been applied in many seismological contexts and, in particular, to downhole seismology, where the interferometry has been used to determine the velocity and attenuation structures in correspondence of instrumented boreholes (e.g. Trampert et al., 1993; Metha et al., 2007; Assimaki, 2008; Parolai et al., 2010). The interferometric approach has been widely used to evaluate the shear wave velocity and attenuation inside the building using earthquake data (e.g. Snieder and Şafak, 2006; Kohler et al., 2007; Nakata et al., 2013; Rahmani and Todorovska, 2013). The deconvolution removes the dependency on the source excitation and, differently from the vibrational approach, the effect of the coupling with the ground (Snieder and Şafak, 2006; Todorovska, 2009). On the other hand, the application of the interferometric approach to ambient vibration is still limited (e.g. Prieto et al., 2010; Nakata and Snieder, 2014). The presence of several internal sources of noise simultaneously acting during the acquisition is the main difference with respect to the interferometry using earthquake data, making the results depending, in general, on the radiation losses at the base of the building (Nakata and Snieder, 2014).

In this study, we apply both OMA and the interferometry approaches to an instrumented 8-story hospital (AHEPA) constructed in the seventies in Thessaloniki (Greece). This RC building has been selected as test site for the European funded REAKT project (http://www.reaktproject.eu/). We first compute the dynamic characteristics of the hospital building to evaluate changes in its vulnerability due to all possible geometrical modifications, mass distributions and material deterioration through time. Traditionally, in seismic vulnerability assessment studies it is implicitly assumed that the structures are optimally maintained during their lifetime neglecting any deterioration effect (e.g. due to aging, pre-existing earthquake damage etc.) that may adversely affect their structural performance under dynamic (or even static) loading (Pitilakis et al., 2014). Therefore, it is of primary importance to identify the real structural conditions and potential pathology of the building. The use of ambient noise measurements for identifying the actual state of the structures is a very attractive technique for that. In the framework of REAKT, a permanent strong motion system was installed for monitoring the building and implementing an early earthquake warning system (EEW) for near real time damage assessment. Since variation in the shear wave propagation induced by an earthquake could be a useful proxy for possible damage detection, in this study we also estimate the shear wave velocity in the building by applying an interferometric approach to ambient vibrations. This waveform approach provides a spatially distribution of physical parameters playing a role in the seismic response of the structure (e.g. shear wave velocity, related to the structural rigidity). Therefore, by merging the interferometric results with the description of the building in terms of normal modes, we get a comprehensive view of the dynamic characteristics of the building.

2 AHEPA hospital: Structural description and permanent instrumentation.

The AHEPA general hospital in Thessaloniki is one of the largest hospitals in northern Greece, located in the campus of Aristotle University. It is a major teaching and research center and part of the National Healthcare System of Greece. The hospital complex consists of 40 buildings of various functions and typologies, 2 electrical substations, a gas distribution network and an underground water supply system. Many of these buildings were built before 1985 and are classified as low seismic code structures. In case of the emergency its central location in the city of Thessaloniki makes it one of the most important medical care centers for an efficient crisis management. The target building hosts both administration and hospitalization activities. It was constructed in 1971 and is considered representative of structures that have been designed according to the old 1959 Greek seismic code (Royal Decree of 1959), where the ductility and the dynamic features of the constructions are ignored. It is an eight story infilled structure and its special feature is that it is composed of two adjacent tall building units that are connected with a structural joint (Figure 1a). UNIT 1 covers a rectangular area of 29m by 16m while UNIT 2 has a trapezoidal cross section of 21m by 27m by 16m. The total height of the building with respect to the foundation level is 28.6m with a constant inter-story height of 3.4m except for the second floor where the height increases to 4.8m due to the presence of a middle floor level which covers only a part of the typical floor plan (Figure 1a). From the structural point of view the buildings force resisting mechanism comprises longitudinal and externally transverse reinforced concrete moment resisting frames (Figure 1a). The columns have variable dimensions along the height of the building starting from 0.45m to 0.70m at the lowest level (basement) and resulting to 0.35m by 0.35m at the upper floor. In the longitudinal direction the outer and inner columns are connected by beams with cross-section of 0.20m by 0.60m and 0.35m by 0.40m respectively. In the transverse direction on the other hand only the exterior columns are connected by beams with dimensions of 0.20m by 0.95m. The presence of beam to beam connections at all floor levels near the staircases and elevator shafts, constitute a complex structural system which is particularly evident in the middle floor where the RC beams are inverted. Reinforced concrete walls are present in both building units, surrounding partially the staircases and the lift shafts; they are not specially detailed for seismic performance. More specifically there are two walls in the transverse and one in the longitudinal direction of UNIT 1 and only one wall in the transverse direction of UNIT 2. The RC walls are 0.20m thick while their length is decreasing significantly along the structures height. Moreover a perimeter reinforced concrete wall with dimensions of 0.20m by 3.00m has been constructed at top of the building. The foundation system consists of simple footings of variable geometries without tie-beams combined partially with a raft foundation. Figure 1b represents a typical cross-section of the hospital with the foundation soil profile and the average shear wave velocities Vs estimated from down-hole tests (Raptakis et al., 1994). The soil consist of a stiff clay with average Vs of about 400-450 m/s, The rock basement (schist) is found at 30 to 35m depth having Vs velocities greater than 750 m/s. The foundation soil at the hospital building can be characterized as soil type B according to EC8 soil classification. Using the SYNER-G taxonomy (Pitilakis et al., 2014) for RC structures to describe the typology of the hospital building, it may be considered typical of high-rise infilled moment resisting frame buildings designed with low seismic code level. The Sosewin (Picozzi et al., 2011) permanent network operates in Ahepa hospital since May 2012. It comprises 13 triaxial accelerometers (MEMS ADXL203 chip) installed on the basement, the first and fourth floors and the roof, as shown in Figure 2. One more accelerometer is installed on the roof of a nearby building and used as bridge node for the data transmission to the two gateways installed outside of the Laboratory of Soil Mechanics, Foundations and Geotechnical Earthquake Engineering.

3 Data and Fourier analysis

Ambient noise measurements were performed on February 12th and 13th, 2013 using seismic stations (i.e. sensor's output proportional to ground velocity). During the first day of experiment, the two building units were instrumented with 39 stations. For each building, two instruments were deployed at each floor, the first on the external side and the second close to the structural joint. Due to restrictions in the logistics, the stations were deployed along the longitudinal corridors, located almost in the middle of the structure (Figures 2 and 3). Two additional stations were deployed at the corners on the roof of the two buildings and one stations outside the structure. The stations were equipped with short period L4C-3D Mark sensors (1Hz natural frequency, three components) connected to Earth Data Logger (EDL PR6-24) 24bit digitizers. The sampling rate was set to 500 samples per second and a gain 10 was used for the pre-amplifier. GPS antennas guaranteed the time synchronizations among the instruments. At four locations, a second station equipped with Güralp broadband seismometers (CMG-40T, 30s natural period) coupled to Reftek recorders (DAS-130) was also deployed for instrumental comparison purposes. In the second day, 51 stations were used (44 EDL and 7 Reftek), adding one station at certain floors. In this study, we analyze the short-period data acquired during the first day of measurements.

Table 1: Serial number and position of all the stations used in the first day ambient noise experiment.

	Unit 1		Unit 2	
Station position	Column 1	Column 2	Column 1	Column 2
Basement	RE-07	RE-03	RE-30	RE-02
1st floor	RE-29	RE-41	RE-01	RE-10
2nd floor	RE-09	RE-31	RE-38	RE-05
3rd floor	RE-22	RE-25	RE-18	RE-14
4th floor	RE-45,T4D50*	RE-39	RE-34	RE-12
5th floor	RE-15	RE-44	RE-26	RE-35,T4K20*
6th floor	RE-17	RE-20	RE-08	RE-33, T4D78*
7th floor	RE-27	RE-23	RE-32	RE-42,T4D49*
Roof	RE-06	RE-24	RE-04	RE-40

Note: * broad-band seismometers, not used in the present study

Figure 4 shows the power spectral densities (PSD) versus time for the station installed outside the building and for two stations installed inside at the first floor and on the roof. The power spectra are computed considering running windows two minutes in length, overlapping by 50% and tapered at both ends (Welch, 1967). The power spectra recorded on the roof clearly indicate the main spectral features (i.e. resonance frequencies) of the coupled building-soil system, and their stability over the analyzed time window. Since the station outside was installed few meters from the structure, the main resonance frequencies of the building are still recognizable in the spectra observed at this station.

The probability density functions (PDF) (e.g. McNamara and Buland, 2004; Marzorati and Bindi, 2006) computed for the power spectral values are shown in Figure 5. The PDF shows that, for frequencies above 1Hz, the level of noise during the measurements is close to the upper limit of Peterson noise model (Peterson, 1993), and well above the self-noise of the instrument (e.g. Strollo et al., 2008a., Strollo et al., 2008b). The narrow spread around the mode values shown by the PDF evaluated for the roof recordings confirms the stability of the spectral features over the analyzed time window. The differences between the 95th and the 5th percentiles of the power spectra distribution ranges between 2 and 10 dB for the longitudinal direction on the roof (between 3 and 10 dB when the vertical component is considered) and between 5 and 11 dB for the station installed in the first floor (from 12 to 24 dB considering the vertical component). This confirms the presence of a more variable noise field inside the building and, in particular, in the first three floors where different entrances to the hospital and connection with adjacent buildings are present.

Figure 6 exemplifies the longitudinal Fourier amplitude spectra (FAS) computed for Unit 1. The average spectra ± one standard deviation are computed considering moving windows 1 minute long and overlapping by 50%. The spectra identify the main resonances of the system at about 1.65 and 1.91 Hz, as will be discussed in the section devoted to the modal analysis. The amplitude of the fundamental peak of resonance increases of about two order of magnitude when moving from the basement to the roof. Except for one station installed in the 6th floor of UNIT 1, which is not considered for further analysis, the FAS are stable over the time of measurements. The FAS for different components are summarized in Figure 7, considering stations installed on the roof, in the basement and outside the building. The peaks of amplification at different frequencies are related to the different modes of vibration, as detailed in the modal analysis presented in the next section.

4 System identification and Operational modal analysis.

In order to predict or modify the response of a structure, an accurate well-known mathematical model is required that represents the dynamics of the structure, the so-called modal model. The process of building a modal model of a physical system based on experimental data is called system identification (Ljung, 1999). The modal model expresses the behavior of a linear time-invariant system as a linear combination of contributions from the different resonance modes of the structure (Parloo, 2003). Based on the knowledge of the systems experimental response (output data) to an excitation source (input data) a parametric modal model can be derived that is defined by a set of modal parameters (eigenfrequencies, mode shapes, damping ratios). There are several deterministic or stochastic techniques that have been developed over the past years that can be used to build the mathematical model of the dynamic structural systems in frequency or time domain based on measured data. A modal model of an artificially excited structure can be obtained based on Experimental Modal Analysis (EMA); however in case of real scale civil engineering structures applying an artificial excitation might be difficult from technical and economical point of view. Therefore, Operational Modal Analysis (OMA) is generally preferred to forced vibration measurements since the same modal parameters can be obtained from vibration data in operational rather than laboratory conditions by modeling the interaction between the structure and its environment (e.g. wind, traffic, etc). Ambient vibration measurements are usually used to perform OMA and to identify the modal parameters of a structure. In contrast to Experimental Modal Analysis, the properties of ambient excitation in Operational or Output- Only Modal Analysis are difficult or impossible to be measured. Therefore stochastic identification techniques have been developed by the assumption that the response is a realization of a stochastic process with unknown white Gaussian noise as input characterized by a flat spectrum in the frequency range of interest. Based on this assumption the excitation input is considered to have the same energy level at all frequencies implying that all modes are excited equally (Van Overschee and De Moor, 1996; Peeters, 2000). There are different stochastic identification techniques to extract the modal parameters of a structural system, namely the parametric and non-parametric methods. In non-parametric methods the modal parameters are estimated directly by post-processing the measured data whereas in the parametric methods the dynamic characteristics are extracted based on a parametric model that is updated to fit the recorded data. To evaluate the dynamic characteristics of the hospital building, namely the natural frequencies and mode shapes, system identification and Operational Modal Analysis were performed using MACEC 3.2 software (Reynders et al., 2011) for the two adjacent building units separately (UNIT 1 and UNIT 2) as well as for the entire hospital building complex, analyzed as one taking into account the interaction of the two building units due to their connection with the structural joint (BUILDING). Operational modal analysis was initially conducted for the horizontal components of the measurements.

The grid of the models was built so that the defined nodes correspond to nodes that have been actually measured. The sensors that were used for the identification process are illustrated in Figures 2 and 3.

Before identification a time window of 1800 sec (30min) was applied and the data were decimated with a factor of 10. The data were filtered with a low-pass anti-aliasing filter with a cut-off frequency of 25Hz and re-sampled at 50Hz reducing thus the number of data from 900000 to 90000 points avoiding thus unnecessary computational burden in the modal analysis where the frequencies of interest are smaller than 25 Hz.

System identification and modal analysis of the structural models under study have been conducted using non-parametric identification techniques, namely the Peak Picking (PP) (Bendat and Piersol, 1993), and the Frequency Domain Decomposition (FDD) (Brincker et al., 2001) methods. The FDD method is considered to be an improved version of the Peak Picking method and consists of decomposing the systems cross power spectral density into its singular values. It is shown that taking the Singular Value Decomposition SVD of the spectral matrix, the latter is decomposed into a set of auto spectral density functions each corresponding to a single degree of freedom (SDOF) system (Brincker et al., 2001).

For the power spectra density estimation of the measured outputs collected from all channels, the correlogram method was applied. In the correlogram approach, the auto and cross-PSDs of one or two quasi-stationary ergodic sequences is estimated as the Laplace transform of the auto or cross correlation functions respectively (Reynders, 2012). In the PP method the averaged normalized power spectral density (ANPSD) is computed and the well separated modes are estimated by picking the peaks in the ANPSD. In the FDD method, the singular values are obtained from the decomposition of the PSD matrix and the modal parameters are estimated by picking the peaks of the first singular value. The results of the modal analyses for the two adjacent buildings analyzed separately (UNIT 1 and UNIT 2) and as one single building (BUILDING) are presented in Figure 8. In Table 2, the eigenfrequencies computed with the two system identification methods are summarized. It is seen that the estimated frequency values for the five well separated modes are very close to each other (practically the same at the first three modes) for the two non-parametric methods applied as well as for the different system models identified.

Table 2: Eigenfrequencies of UNIT 1, UNIT 2 and BUILDING estimated using the nonparametric system identification techniques

		UNIT1		UNIT2		BUILDING	
Mode	Mode type	PP [Hz]	FDD [Hz]	PP [Hz]	FDD [Hz]	PP [Hz]	FDD [Hz]
1	Coupled translational	1.65	1.65	1.65	1.65	1.65	1.65
2	Coupled translational	1.91	1.9	1.91	1.91	1.91	1.91
3	Torsional	2.33	2.33	2.35	2.35	2.35	2.35
4	Coupled translational	3.5	3.5	3.58	3.58	3.54	3.58
5	Coupled translational	5.2	5.2	5.2	5.22	5.2	5.2

Similar orders and shapes of the modes are estimated for the different system models as illustrated in Figures 9, 10 and 11. This implies that the dynamic interaction of the two adjacent buildings due their connection with the structural joint is reflected on the measured outputs, and the dynamic characteristics of the complex hospital building is possible to be captured by monitoring and analyzing the two adjacent building units separately. Moreover the fact that frequencies and mode shapes are identical for both units may be attributed to their similar structural configuration. The building is exhibiting coupled sway and torsional modes in the frequency range of interest which is expected in case of geometric and structural irregularities or eccentricities between the center of mass and center of rigidity. The highly coupled obtained mode shapes confirm the complex vibrational characteristics of the building especially for the first two identified frequencies. Figure 12 represents indicatively for UNIT 1 the contribution of the transverse, longitudinal and torsional motion in the first two modes. It should be noted herein that a comparison with the modal identification results extracted using the SSI-Stochastic Subspace Identification method (Van Overschee and De Moore, 1996) confirms the reliability of the identified frequencies and mode shapes with the nonparametric approaches presented in this paper (Karapetrou et al. 2014).5 Interferometry

In this section, we determine the building impulse response function (IRF) by following a waveform approach based on seismic interferometry. Differently from the vibrational approach, that describes the soil-building system as a whole, deconvolution interferometry allows us to get an insight about the spatial distribution inside the building, using parameters, like the shear wave velocity, that are connected to the dynamic characteristics of the structure alone. Assuming a linear and time invariant system, the interferometric approach is based on deconvolving the signal $u_{ref}(t)$ recorded at a reference location from the signal $u(t)$ recorded at a generic location. In the Fourier domain, the deconvolution can be written as (e.g. Snieder and Şafak, 2006)

$$D(\omega) = \frac{\hat{u}(\omega)}{\hat{u}_{ref}(\omega)} \tag{1}$$

where the symbol ^ indicates the Fourier transform and $\omega=2\pi f$ is the angular frequency. Considering the ill-posed nature of the deconvolution, the spectral ratio has to be regularized. Among different possible regularization schemes (e.g. Bertero and Boccacci, 1998; Bindi et al., 2010), we apply the so-called water-level regularization (e.g. Wiggins and Clayton, 1976)

$$\mathrm{D}(\omega) = F(\omega)\hat{u}(\omega) \tag{2}$$

$$F(\omega) = \frac{\hat{u}^*_{ref}(\omega)}{\left|\hat{u}_{ref}(\omega)\right|^2 + \varepsilon} \tag{3}$$

where ε is the regularization parameter which controls the degree of filtering applied to the spectral ratio to stabilize the retrieved Impulse Response Function $\mathrm{D}(\omega)$. In this study, the values of ε are given as percentage (hereinafter referred to as α) of the average spectral power. The vertical propagation of the seismic waves in the building can be easily described if assuming a shear-beam model (Iwan,1997). Following Snieder and Şafak (2006) the deconvolution of the motion recored at a generic height z with respect to the motion recorded at the highest floor $z=H$ is given by

$$T(z,\omega) = \frac{1}{2}\left[e^{ik(z-H)}e^{-\gamma|k|(z-H)} + e^{ik(H-z)}e^{-\gamma|k|(H-z)}\right] \tag{4}$$

where k is the wavenumber $k=\omega/c$, c is the shear wave velocity of the building, and γ is the viscous damping related to the quality factor Q by $\gamma=1/2Q$. $T(z,\omega)$ describes the response of the system when a virtual source is acting at the top of the building at $t=0$. The first term in equation (4) describes an acausal (i.e. $t<0$) up-going wave, while the second term describes the causal down-going wave. When the deconvolution is performed with respect to the motion at the base of the building, the impulse response function is given by (Snieder and Şafak, 2006)

$$B(z,\omega) = \frac{e^{ikz}e^{-\gamma|k|z} + e^{ik(2H-z)}e^{-\gamma|k|(2H-z)}}{1+e^{2ikH}e^{-2\gamma|k|H}} \tag{5}$$

Expressing the denominator in term of geometric series, equation (5) can be rewritten as (Snieder and Şafak, 2006)

$$B(z,\omega) = \sum_{n=0}^{\infty}(-1)^n\left[e^{ik(z+2nH)}e^{-\gamma|k|(z+2nH)} + e^{ik(2(n+1)H-z)}e^{-\gamma|k|(2(n+1)H-z)}\right] \tag{6}$$

where the summation index n counts the number of bounces off the base. $B(z,\omega)$ is a causal function composed by an infinite sum of up-going and down-going waves. Both $B(z,\omega)$ and $T(z,\omega)$ are independent on the reflection coefficient at the base of the building, that is they are not depending on the coupling with soil. For a detailed discussion about how the deconvolution is changing the boundary conditions with respect to those for the original wave field, see (Snieder and Şafak, 2006).

Many studies applied equations (4) and (5) to extract the building response using earthquake data. When ambient vibrations are considered, the presence of multiple internal sources simultaneously exciting the building introduces a dependence of the deconvolved waveforms on the ground coupling, in particular for the attenuation (Nakata and Snieder, 2014). To obtain stable deconvolved waveforms, a stacking procedure is applied to the deconvolution computed for several time windows (Prieto et al., 2010; Nakata and Snieder, 2014). In this study, we analyze 1 hour of ambient vibration.

5.1 Deconvolution and parameters selection.

The scheme applied to compute the IRFs is exemplified in Figure 13, considering three sensors, installed in the basement, on the 4th floor, and on the roof (Figure 3). Panel (a) shows the moving windows running over the noise records, with a duration of about 32s, overlapping for 50% and cosine-tapered at both ends. The spectra computed for each window (panel b) are lowpass filtered and used to computed the regularized spectral ratio given by equation (1). The spectrum at the reference station (located on the roof in this example) is used to construct the filter $F(\omega)$ given by equation (3), shown in panel (c). The shape of the filter is determined by the spectrum at the reference station and the degree of filtering is controlled by the regularization parameter ε. The filter applied to the spectra computed at the different floors provide the impulse response function between each considered sensor and the reference one, as shown in Figure 14 both in the frequency and time domains. The IRFs in the time domain are used to estimate the average shear wave velocity by measuring the time lag τ between the a-causal and causal pulses. In particular, the average velocity between the floor at height z and H (roof) is given by $v=D/\tau$ where $D=2(H-z)$. The average velocity is estimated using a least-squares fit by considering the time lag measured at different floors. The amplitude ratio A_-/A_+ between the a-causal (A_-) and causal (A_+) pulses can be used to estimate the quality factor Q using $1/2Q=\ln(A_-/A_+)/\omega_{eff}\tau$, where ω_{eff} is the effective bandwidth.

Both the regularization parameter and the passband of the filter applied to the original waveforms affect the resolving power of the restored IRFs. To choose the regularization parameter, we analyzed the spectra of the IRF obtained at $z=H$, i.e. the motion recorded at the top deconvolved with itself, considering different values for α . As expected, we observed that an increase of α reduces the bandwidth of the IRF and we found that $\alpha=10^{-3}$ is a good compromise between stability and resolution for the inverse problem analyzed in this study.

Finally, to evaluate the impact of the selected filter on the average velocity estimation for a single station. We compared the estimated velocities obtained for different low-pass corner frequencies, from 10 to 50 Hz. Considering $\alpha=10^{-3}$, the difference of the velocity estimates for low-pass frequencies larger than 20 Hz is about 5 m/s. In the remainder of the paper, we show the results obtained filtering the data over the band [0.1-20]Hz.

5.2 Velocity and attenuation

Figure 15 shows the IRFs obtained for the three components of the motion of UNIT 2 using as reference the motion recorded at the roof (equation (4)). The compressional P-waves characterize the IRF along the vertical component. Although a larger frequency band of [0.1-50] Hz has been used for this component to better resolve the up-going and down-going pulses, the wavelength associated to the P-wave is still too long to measure reliable the time delay between the pulses. In the remainder of the paper, the results for the vertical component are not further discussed.

The IRFs for the basement and for the first two floors (gray traces) show more complex patterns than the IRFs for the upper floors (black traces). The latter are mainly characterized by the up and down-going pulses. We ascribe the complex structure of the IRFs for the first three levels to the complex distribution of internal sources within these levels. In particular, the main hospital entrance is located at the second floor on the east side, while service entrances are located both at the basement and on the first floor. Due to structural changes, e.g. the increase of floor height on the second floor, internal reflection may also contribute to the complex structure of the IRFs, not only in the lower layers. Moreover, the first three levels are connected to adjacent buildings with structural joints in all four directions, with corridors connecting the different buildings. The short time of data acquisition (from one to few hours) does not mitigate the effect of these sources of noise and stacking over longer time periods are probably needed to enhance the IRFs.

The time lag between the propagation pulses at different floors is used to estimate the shear wave velocity. For each horizontal component, the estimates are performed separately for each of the four columns described in Figure 3, and the results are shown in Figure 16. Using a least squares fit either considering the columns separately or grouping all the results together, the slowness (χ), which corresponds to the slope of the line, is determined. The values of the height are assumed to be error free and only an error for the lag time is assumed. Only the observation between the third and sixth floors are considered for performing the linear fit, since a significant interference between up-going and down-going waves can occur in the IRF for the seventh floor. The velocities are calculated as $v=1/\chi$ and listed in Table 3. The given errors are standard deviations calculated from the standard deviations of the slownesses. The average velocities are estimated as $v_{\mathrm{longitudinal}}$=200m/s and $v_{\mathrm{transverse}}$=276m/s for the longitudinal and transverse direction, respectively. The velocities determined for the four columns separately, are similar to the average velocities. The building can be assumed as homogeneous in the horizontal directions.

Table 3: Propagation shear wave velocities

	1st column	2nd column	3rd column	4th column	all columns
$v_{transverse}$ [m/s]	275± 7	271±14	286±14	271±12	276±6
$v_{longitudinal}$ [m/s]	195±10	191±11	205±11	209± 13	200±6

The different average velocities for the transverse and longitudinal components are also visible in the IRFs in Figure 15. Although more uncertain due to the noisy IRFs, the delays estimated at the first three layers suggest higher shear velocities for both components in this part of the structure. The velocity for the first floors is estimated by matching the empirical IRFs and the theoretical ones, obtained considering a shear-beam model (e.g. Rahmani and Todorovska, 2013) and varying the model characteristics until the best fit is obtained. The code developed by Wang (1999) is considered for the determination of the vertical propagation of SH-waves in a layered medium. The soil profile described in Figure 1b is considered at the base of the building. The building is divided into three parts: one from the basement to the second floor, one from the second to the third floor and the third from the third floor to the roof. Since the third floor differs in height and structure from the other floors, it is considered as one layer. For the upper layer the velocities obtained by the least squares fit (Table 3) are used. The quality factor is fixed to $Q=60$ to reasonably reproduce the amplitudes of the IRFs, and density to $\rho=600 Kg/m^3$, as estimated based from the mass of the building and the corresponding volume. It is worth noting that the simulation aims at estimating the shear wave velocities of the lowest layers by finding the best match between the arrival times of theoretical and empirical up-going and down-going pulses. An optimized modeling of the pulse shapes and amplitude is beyond the scope of the present work. The obtained velocities for the three layers (Figure 17) are given in Table 4.

Table 4: Wave velocities obtained for the shear-beam model (see Figure 17).

	1st layer	2nd layer	3rd layer
$v_{transverse}$ [m/s]	1000	400	276
$v_{longitudinal}$ [m/s]	500	200	200

For all layers and hence, the whole building, the propagation velocity is higher in the longitudinal than in the transverse direction. The velocity decreases with the height of the building, since the stiffness decreases as well.The velocity changes between the second and the third floor for both components which can be explained by the changes in construction. Furthermore, the velocity decreases for the transverse direction between the 2nd and the 3rd layer, no change in velocity is observed for the longitudinal direction.

The seismic waves attenuate during the propagation inside the building due to intrinsic attenuation, scattering and radiation losses. We analyze the IRFs obtained through the deconvolution interferometry for evaluating the intrinsic attenuation, which quantifies the anelastic dissipation of the building’s motion and breaks the symmetry of the IRF for time reversal (e.g. Newton and Snieder, 2012).

Following Parolai et al. (2010), the transfer function between a generic floor inside AHEPA and the roof (see equation 4) is fit in the Fourier domain with the theoretical model (e.g. Şafak, 1997):

$$|T(z,\omega)| = \frac{\sqrt{1 + \frac{e^{-4\pi f\tau}}{Q_S} + 2\frac{e^{-2\pi f\tau}}{Q_S} cos(4\pi f\tau)}}{2\frac{e^{-\pi f\tau}}{Q_S}} \tag{7}$$

where the quality factor Q_S is related to the damping coefficient $\zeta=1/2Q$. A grid search procedure is applied over the quality factor Q_S and the travel time τ, in order to minimize the root mean square error between the logarithm of the empirical and theoretical spectra. The model in equation (7) reproduces the trough in the spectrum generated by the negative interference (e.g., see Figure 13). The positions of the troughs are controlled by the travel time while the intrinsic attenuation controls the amplitude of the troughs and their attenuation with frequency. As already discussed in Parolai et al. (2010), the role played by Q_S in the cost function decreases with increasing Q_S. Therefore, by fitting the model of equation (7) to the empirical spectra, we obtain a reliable estimate for the minimum quality factor which allows us to reproduce the main spectral features.

Considering the complex patterns characterizing the transfer functions for the three lowest floors, model (7) is applied considering the motion recorded at the fourth floor for the transverse component and at the fifth floor for the longitudinal one. In the grid search, τ is allowed to assume values in the range ±10 % with respect to the empirical values measured from the IRF, while the range of variability for Q_S is fixed to 1-100. It is worth noting that the quality factor is considered frequency independent and is not associated to a specific mode but describing the overall attenuation of the system over the frequency range used for the spectral fit (i.e. 1-15 Hz). The results are shown in Figure 18. The quality factors for the best fit models are Q=54 and Q=25 for the longitudinal and transverse components, respectively. The grid search results for different Q and τ values are shown in panel c. The position of the minimum misfit is marked by a white cross. The cross sections (panels d and e) confirm that the cost function has a steep gradient toward lower Q values and an almost flat variability toward higher Q. A visual inspection of the fit result (panel a and b) confirms that the fit is satisfactory for both the longitudinal and transverse directions.

6 Discussion and Conclusions

In the present paper, the dynamic response of an eight-story RC building, belonging to the AHEPA general hospital complex in Thessaloniki (Greece), has been investigated and evaluated using ambient noise measurements. The special feature of the building is that it is composed of two adjacent tall building units that are connected with a structural joint. It was selected within the framework of European funded REAKT project as representative of high-rise infilled moment resisting frame buildings in Europe designed with low seismic code level; the aim is to implement a real-time permanent monitoring system to evaluate its risk for various earthquake scenarios and generate real-time risk estimates. Ambient vibration measurements were used for system identification and operational modal analysis to extract the natural frequencies and mode shapes for the two adjacent buildings first separately, and then for the entire building analyzed as one single structure taking into account the interaction of the two building units. The estimated modal parameters for five clearly identified modes were similar for the applied non-parametric identification methods (Peak Picking and Frequency Domain Decomposition methods) as well as for the different system models analyzed, implying that it is possible to capture the dynamic characteristics of the hospital building by monitoring and analyzing the two adjacent buildings separately. The identified modal characteristics indicate that the first two modes, corresponding to f_1=1.65 Hz and f_2=1.91 Hz respectively, are mainly translational along the transverse direction, although a significant coupling exists. The first two mode shapes are similar; however the contribution of the torsional motion is higher in the second mode. For the third (f_3=2.35 Hz), fourth (f_4=3.58 Hz) and fifth (f_5=5.2 Hz) frequencies, mode shapes are clearer and correspond to a torsional and two translational modes in the longitudinal direction, respectively. The modal characteristics will be used in a future stage of the research to calibrate the numerical model of the building and derive fragility curves that reflect the actual state and behavior of the building subjected to seismic loading.

The ambient vibration recordings were also used to perform interferometric analyses to investigate the shear wave propagation in the building and the intrinsic attenuation. The average velocities along the longitudinal and transverse directions are about (200± 6) m/s and (276± 6) m/s, respectively, while the quality factors estimated for the two components are 54 and 25, respectively. The availability of a couple of earthquakes recorded inside the building allows to compare the interferometric results from ambient vibration and earthquakes, as shown in Figures 19 and 20. The time lags between the a-causal and causal pulses observed at first and fourth floors are in good agreement with the ambient vibration results. Differently from the ambient vibration case, the deconvolution with earthquake data provides a reliable IRF also at the basement. The quality factor estimated for the analyzed earthquake is 40 and 28 along the longitudinal and transverse component (Figure 20), in good agreement with the noise results.

The distribution of the shear wave velocity estimated from interferometric analysis using both ambient noise and earthquake recordings indicates that the structure is stiffer at the base and along the transverse direction. The increased stiffness at the base building is expected due to the fact that the basement is partially embedded (in one side only, see Figure 1) and because the dimensions of the reinforced concrete elements (columns) are progressively decreasing along its height. However, the higher stiffness in the transverse (shorter) direction is not matching with the results of operational modal analysis. According to the modal analysis, the fundamental mode shape, although highly coupled, corresponds to a mode that is mainly translational along the transverse direction implying that in this direction the building is expected to be more flexible. Considering the complex vibration characteristics of the building the differences may be due to a number of reasons, which undergo further investigation in order to reach conclusions. For example, considering the complex vibrational characteristics of the building, further investigations are needed to conciliate the waveform and vibrational outcomes. In order to further validate the results of system identification and operational modal analysis, a comparative study between non-parametric and parametric identification techniques is needed, including also estimation of damping ratios. Further analysis is also required taking into account the vertical component to interpret its high amplitude and investigate potential effects of rocking on the building. Since deconvolution interferometry with earthquake data provides building responses independent from soil-structure coupling (Snieder and Safak, 2006), the data set of earthquakes recorded by the permanent network installed in the building can be exploited in future studies to evaluate the importance of the soil-structure interaction.

In order to enhance the reliability and robustness of the results, and to come up with final conclusions regarding the dynamic characteristics of the complex building, further investigation studies are currently underway using both ambient noise and earthquake recordings. The modal identification results will be used in the framework of REAKT to update and better constrain the initial finite element models of the hospital building units aiming to the vulnerability assessment of the building considering its actual state, taking into account potential structural degradation due to time (it is already 40 years old), possible structural damages, changes in geometry and mass distribution. It is concluded that ambient vibration measurement in combination with interferometry analysis of the wave propagation from the same ambient noise recording within the building skeleton an be used to yield more reliable models with respect to their real condition on the basis of real-time risk assessment and pre- or/and post-event fragility updating.

Acknowledgements

The ambient vibration survey in AHEPA was performed using the seismic instruments provided by the Geophysical Instrument Pool Potsdam (GIPP) and supported by the REAKT (Strategies and tools for Real Time EArthquake RisK ReducTion) project. The staff of AHEPA hospital is acknowledged for their kind support during the experiment. Comments from two anonymous Reviewers are also acknowledged.

References

Aki K (1957). Space and time spectra of stationary stochastic waves with special reference to microtremors. *Bulletin Earthquake Research Institute*; **35**: 415-457.

Assimaki D, Li W, Steidl JH, Tsuda K. (2008) Site amplification and attenuation via downhole array seismogram inversion: a comparative study of the 2003 Miyagi-Oki aftershock sequence. *Bulletin of the Seismological Society of America* ; **98**: 301330.

Bendat JS, Piersol AG.(1993) Engineering Applications of Correlation and Spectral Analysis.

John Wiley & Sons
Bertero M, Boccacci P. (1998) Introduction to Inverse Problems in Imaging. *IOP Publishing Bristol*.
Bindi D. Parolai S, Picozzi M, Ansal A. (2010) Seismic input motion determined from a surface-downhole pair of sensors: a constrained deconvolution approach. *Bulletin of the Seismological Society of America*; **100**: 13751380.
Brincker R, Zhang L, Andersen P. (2001) Modal identification of output only systems using frequency domain decomposition. *Smart Materials and Structures*; **10**:441445.
Brownjohn JMW (2003). Ambient vibration studies for system identification of tall buildings. *Earthquake Engineering Structural Dynamics*; **32**: 71-95.
Carder DS. (1936) Observed vibration of buildings. *Bulletin of the Seismological Society of America*;**26**:24577.
Chopra AK.(1996) Modal analysis of linear dynamic systems: physical interpretation, *Journal of Structural Engineering*; **122**: 517-527.
Wiggins RW, Clayton RA. (1976) Source shape estimation and deconvolution of teleseismic bodywaves. *Geophysical Journal of the Royal Astronomical Society*; **47**: 151-177
Clearbout JF. (1968) Synthesis of a layered medium from its acoustic transmission response. *Geophysics*; **33**: 264-269.
Davison C. (1924) Fusakichi Omori and his work on earthquakes. *Bulletin of the Seismological Society of America*; **14**:240255.
Guéguen P, Michel C, Le Corre L. (2007) A Simplified Approach for Vulnerability Assessment in Moderate-to-low seismic hazard Regions: Application to Grenoble (France). *Bulletin of Earthquake Engineering*; **5**:467490.
Holcomb LG. (1989) A direct method for calculating instrument noise levels in side-by-side seismometer evaluations. *U.S. Geological Survey Open File Report*: 89-214
Housner GW, Brady AG. (1963) Natural periods of vibration of buildings. *Journal of the Engineering Mechanics Division*; **89**:3165.
Ivanović SS, Trifunac MD, Todorovska MI.(2000) Ambient vibration tests of structuresA review. *Journal of Earthquake Technology*; **37**: 165197.
Iwan WD.(1997) Drift spectrum: measure if demand for earthquake ground motions. *Journal Structural Engineering*; **123**: 367404.
Jaishi B, Ren WX. (2005) Structural finite element model updating using ambient vibration test results. *Journal of Structural Engineering*; **131**: 617-628
Kanai K. (1965)Some new problems of seismic vibrations of a structure. *Proceedings of the 3rd World Conference on Earthquake Engineering*, Auckland and Wellington, New Zealand.
Karapetrou Sotiria, Manakou Maria, Lamprou Despoina, Kotsiri Sofia and Pitilakis Kyriazis (2014). “Real-time” seismic vulnerability assessment of a high rise RC building using field monitoring data, *Second European conference on Earthquake Engineering and Seismology*, Istanbul, August 2014.
Kohler MD, Heaton TH, Bradford SC. (2007) Propagating waves in the steel, moment-frame Factor building recorded during earth- quakes. *Bulletin of the Seismological Society of America*; **97**: 13341345.
Ljung L. (1999) System identification: Theory for the User. *Prentice Hall, Upper Saddle River, 2nd Edition*
Lobkis OI, Weaver RL. (2001) On the emergence of the Greens function in the correlations of a diffuse field. *Journal of the Acoustical Society of America*; **110**: 30113017.
Marzorati S, Bindi D.(2006) Ambient noise levels in north central Italy.*Geochemistry Geophysics Geosystems*;**7**: Q09010, doi 10.1029/2006GC001256.
McNamara DE, Buland RP. (2004) Ambient noise levels in the continental United States. *Bulletin of the Seismological Society of America*;**94**: 15171527.
Mehta K, Snieder R, Grazier V. (2007) Downhole receiver function: a case study. *Bulletin of*

the Seismological Society of America ; **97**: 13961403.

Michel C, Guéguen P, Bard PY.(2008) Dynamic Parameters of Structures extracted from Ambient Vibration Measurements: An Aid for the Seismic Vulnerability Assessment of Existing Buildings in Moderate Seismic Hazard Regions. *Soil Dynamics and Earthquake Engineering*; **28**:593604.

Michel C, Guguen P, Causse M. (2012) Seismic Vulnerability Assessment to Slight Damage based on Experimental Modal Parameters. *Earthquake Engineering and Structural Dynamics*; **41**: 81-98.

Nakata N, Snieder R, Kuroda S, Ito S, Aizawa T, Kunimi T. (2013) Monitoring a building using deconvolution interferometry, I: Earthquake-data analysis. *Bulletin of the Seismological Society of America*; **103**:1662 1678

Nakata N, Snieder R. (2014) Monitoring a building using deconvolution interferometry, II: Ambient vibration analysis. *Bulletin of the Seismological Society of America*;**104**: 204-213.

Newton C, Snieder R. (2012) Estimating intrinsic attenuation of a building using deconvolution interferometry and time reversal. *Bulletin of the Seismological Society of America*; **5**; 2200-2208.

Parloo E. (2003) Application of Frequency Domain System Identification Techniques in the Field of Operational Modal Analysis. *PhD Dissertation, VRIJE Universiteit, Brussel*

Parolai S, Bindi D, Ansal A, Kurtulus A, Strollo A, Zschau J. (2010) Determination of shallow S-wave attenuation by down-hole waveform deconvolution: a case study in Istanbul (Turkey), *Geophysical Journal International*; **181**: 1147-1158

Peeters B, De Roeck G. (1999) Reference-based stochastic subspace identification for output-only modal analysis. *Mechanical Systems and Signal Processing*; **13**: 855-878.

Peeters B. (2000) System Identification and Damage Detection in Civil Engineering. *PhD thesis, Department of Civil Engineering, K.U.Leuven*

Peterson J. (1993) Observations and modeling of background seismic noise, i*U.S. Geological Survey Open File Report*: 93-322.

Picozzi M, Parolai S, Mucciarelli M, Milkereit C, Bindi D, Ditommaso R, Vona M, Gallipoli MR, Zschau J. (2011) Interferometric Analysis of Strong Ground Motion for Structural Health Monitoring: The Example of the LAquila, Italy, Seismic Sequence of 2009. *Bulletin of the Seismological Society of America*; **101**: 635651.

Pitilakis KD, Karapetrou ST, Fotopoulou SD. (2014) Consideration of Aging and SSI effects on Seismic Vulnerability Assessment of RC Buildings. *Bulletin of Earthquake Engineering*; (article in press)

Prieto GA, Lawrence JF, Chung AI, Kohler MD. (2010) Impulse response of civil structures from ambient noise analysis,*Bulletin of the Seismological Society of America*; **100**; 23222328.

Rahmani MT, Todorovska MI. (2013) 1D system identification of buildings from earthquake response by seismic interferometry with waveform inversion of impulse responses - method and application to Millikan Library. *Soil Dynamics and Earthquake Engineering*; **47**: 157-174.

Raptakis DG, Anastasiadis AJ, Pitilakis KD, Lontzetidis K. (1994) Shear wave velocities and damping of Greek natural soils, *Proceeding of the 10th Conference on Earthquake Engineering*; **1**: 477-482.

Reynders E, Schevenels M, De Roeck G. (2011) MACEC 3.2: A Matlab toolbox for experimental and operational modal analysis-User’s manual. *Katholieke Universiteit, Leuven*

Reynders E. (2012) System Identification Methods for (Operational) Modal Analysis: Review and Comparison. *Archives of Computational Methods in Engineering*; **19**; 51-124

Şafak E. (1997) Models and methods to characterize site amplification from a pair of records. *Earthquake Spectra*, EERI ;**13**: 97-129.

Snieder R, Şafak E. (2006) Extracting the building response using interferometry: theory and applications to the Millikan Library in Pasadena, California. *Bulletin of the Seismological Society of America*;**96**: 586598.
Strollo A, Parolai S, Jäkel K.H., Marzorati S, Bindi D. (2008a) Suitability of short-period sensors for retrieving reliable H/V peaks for frequencies less than 1 Hz.*Bulletin of the Seismological Society of America*; **98**: 671681
Strollo A, Bindi D, Parolai S, Jäckel K-H (2008b) On the suitability of 1 s geophone for ambient noise measurements in the 0.1–20Hz frequency range: experimental outcomes, Bull Earthquake Eng 6, 141-147
Teughels A.(2003) Inverse modeling of civil engineering structures based on operational modal data. *PhD thesis, Katholieke Universiteit of Leuven*.
Todorovska MI. (2009) Soil-structure system identification of Millikan library northsouth response during four earthquakes (1970-2002): what caused the wandering of the observed system frequencies. *Bulletin of the Seismological Society of America*; **99**: 626635
Todorovska MI, Trifunac MD. (1990) A note on the propagation of earthquake waves in buildings with soft first floor. *Journal of Engineering Mechanics*;**116**:892-900
Trampert J, Cara M, Frogneux M. (1993) SH propagator matrix and Qs estimates from borehole- and surface-recorded earthquake data. *Geophysical Journal International*; **112**: 290299.
Trifunac MD. (1972) Comparisons Between Ambient and Forced Vibration Experiments. *Earthquake Engineering and Structural Dynamics*; **1**: 133-150.
Van Overschee P, De Moor B. (1996) Subspace Identification for Linear Systems: Theory-Implementation-Applications. *K.U.Leuven Academic Publishers*
Ventura C, Liam Finn W-D, Lord JF, Fujita N. (2003) Dynamic characteristics of a base isolated building from ambient vibration measurement and low level earthquake shaking. *Soil Dynamics Earthquake Engineering*; **23**:31322.
Wapenaar K. (2004) Retrieving the elastodynamic Greens function of an arbitrary inhomogeneous medium by cross correlation. *Physical Review Letters*; **93**; 254301
Wang R., (1999). A simple orthonormalization method for stable and efficient computation of Greens functions. *Bulletin of the Seismological Society of America*; **89**: 733741.
Welch, P.D. (1967) "The Use of Fast Fourier Transform for the Estimation of Power Spectra: A Method Based on Time Averaging Over Short, Modified Periodograms", IEEE Transactions on Audio Electroacoustics, AU-15, 70–73.

Figure captions

Figure 1: (a) Typical floor plan and middle floor with the structural joint and (b) typical soil profile in correspondence of AHEPA hospital building.

Figure 2: Floor plans of the basement, the first and fourth floor and the roof. The permanent strong motion (code SB, S0 or SC) and temporary seismometers (code RE or T4) are also shown.

Figure 3: Sections A-A and B-B along the longitudinal and transverse direction of the hospital building with the temporary instrumentation.

Figure 4: Longitudinal power spectra densities (PSD) computed for the stations installed outside (left panel), on the 1st floor (middle panel) and on the roof (right panel). The power spectral values are expressed in decibel (dB) with respect to velocity $[(m/s)^2/Hz]$.

Figure 5: Probability Density Function (PDF) for the stations installed outside the building (bottom), on the first floor (middle) and on the roof (top). The longitudinal components are shown on the left, the vertical ones on the right. The power spectra are expressed in decibel (dB) with respect to velocity $[(m/s)^2/Hz]$. The black curve identify the 5-th and 95-th percentiles of the distributions. The New High Noise Model and the New Low Noise Model of Peterson (1993) are shown as gray lines. The self noise of the instrument (sensor and digitizer), shown by the blue curve in the longitudinal plots, was derived by coherency measurements (Holcomb, 1989).

Figure 6: Fourier Amplitude Spectra (FAS) for the longitudinal component, considering the instruments installed along the external (left panels) and internal (right panels) vertical lines of Unit 1 (see Figure 3). The black line indicates the mean value, $\pm 1\sigma$ is shown in gray.

Figure 7: Fourier amplitude spectra (mean $\pm 1\sigma$) for the three components of motion computed for stations installed on the roof (a and b are the two columns in Unit 1; e and f in Unit 2) and in the basement (c and d in Unit 1; g and h in Unit 2). The spectra for the station installed outside AHEPA are shown in panel i.

Figure 8: Modal identification using the Peak Picking (top) and the Frequency Domain Decomposition (bottom) applied to ambient noise measurements. The first five modes are indicated with red circles (top panels) and dashed lines (bottom panels).

Figure 9: Mode shapes corresponding to the first five identified frequencies for UNIT 1.

Figure 10: Mode shapes corresponding to the first five identified frequencies for UNIT 2.

Figure 11: Mode shapes corresponding to the first five identified frequencies for BUILDING.

Figure 12: Contribution of the lateral components in the first two modes along the longitudinal and transverse direction for UNIT 1.

Figure 13: Sketch of the applied deconvolution scheme. (a): velocity recorded at three different locations inside the building; the signal in gray indicates a moving time window used to compute the Fourier spectrum. (b): Fourier amplitude spectra (black) computed for a given time window and filtered spectra (gray). (c): spectrum on roof and filter functions for different values of α (see equation (3))

.

Figure 14: Example of deconvolution results (IRF), computed with respect to the motion on the roof for three different locations within the building. (left) IRFs in frequency domain; (right) IRFs in time domain.

Figure 15: Deconvolution for UNIT 2 with respect to the motion on the roof, considering the three components. The black traces are characterized by the up-going and down-going waves, the gray traces show a more complex pattern. The black lines indicate the average velocities obtained by the interferometry. The dashed gray lines represent the velocities estimated by a comparison of empirical and theoretical IRFs.

Figure 16: Travel times between the propagation pulses at different floors versus distance to the roof, considering the transverse (left) and longitudinal (right) components. In the uppermost panels, the slowness χ is estimated using a least squares fit, considering the columns separately. Each line indicates the slowness of one column. In the lower panels, the slowness is determined grouping the results of all columns.

Figure 17: Comparison between empirical IRFs and those computed for the shear-beam model, considering the longitudinal (left) and the transverse (right) directions. For the uppermost floors (3rd floor-roof), the velocities estimated in Figure 16, and listed in Table 3, are used.

Figure 18: Results for Q estimation using ambient vibration for the longitudinal (left) and transverse (right) directions. (a) Comparison between the empirical (black) and the best fit model IRF spectra (gray); (b) grid search results for different travel time-Q values. The minimum misfit is indicated by a white cross. (c) Cross section along the Q values for the travel time of the minimum misfit function (white line in b). The minimum of Q is indicated by a gray point.

Figure 19: IRFs for noise (gray) and earthquakes (black) for the longitudinal (left) and the transverse component (right). Recordings of two different earthquakes (Volvi earthquake of 11 October 2013; Mw 4.2; distance 38 km and Cephalonia earthquake of 26 January 2014; Mw 6.1; distance 350 km) are used.

Figure 20: Results for Q estimation for the longitudinal (left) and transverse (right) directions, using a recording of the Cephalonia earthquake. (a) Comparison between the empirical (black) and the best fit model IRF spectra (gray); (b) grid search results for different travel time-Q values. The minimum misfit is indicated by a white cross. (c) Cross section along the Q values for the travel time of the minimum misfit function (white line in b). The minimum of Q is indicated by a gray point.

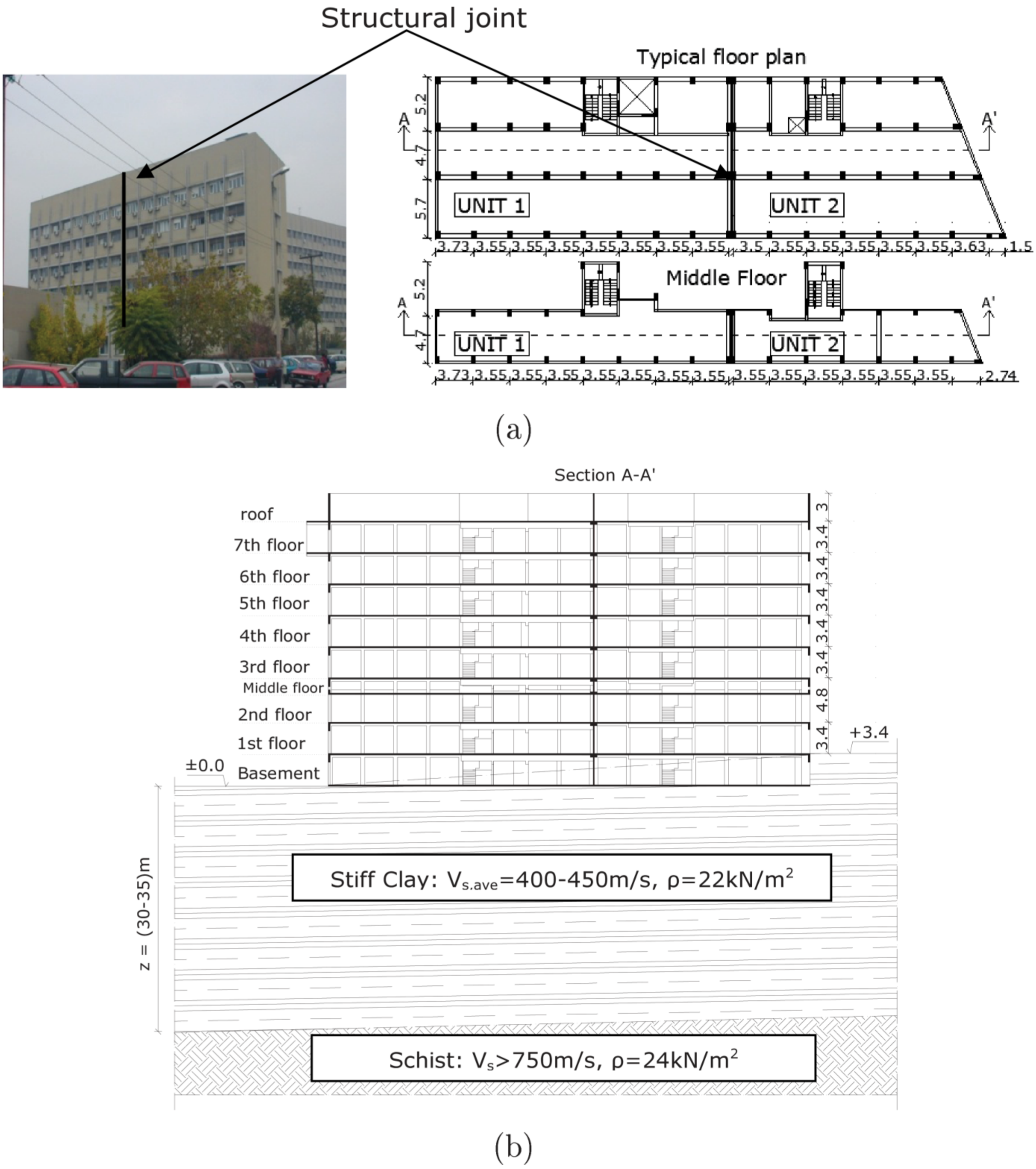

Figure 1 (a) Typical floor plan and middle floor with the structural joint and (b) typical soil profile in correspondence of AHEPA hospital building.

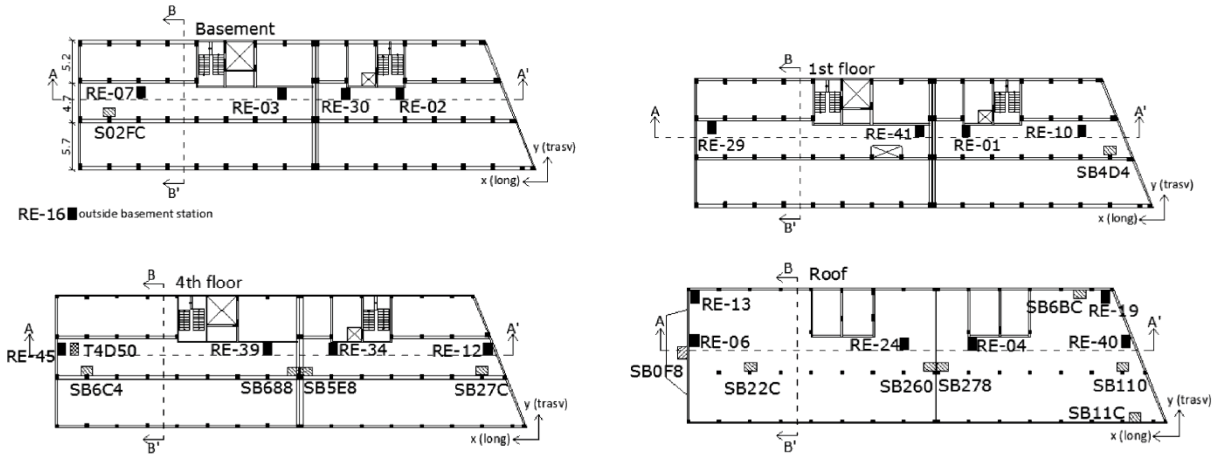

Figure 2: Floor plans of the basement, the first and fourth floor and the roof. The permanent strong motion (code SB, S0 or SC) and temporary seismometers (code RE or T4) are also shown.

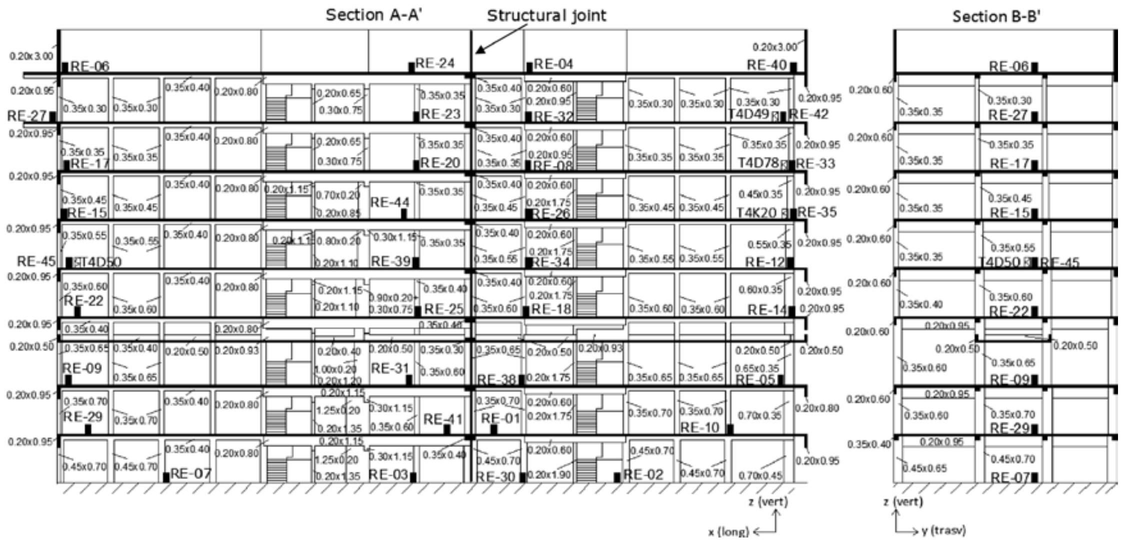

Figure 3: Sections A-A and B-B along the longitudinal and transverse direction of the hospital building with the temporary instrumentation.

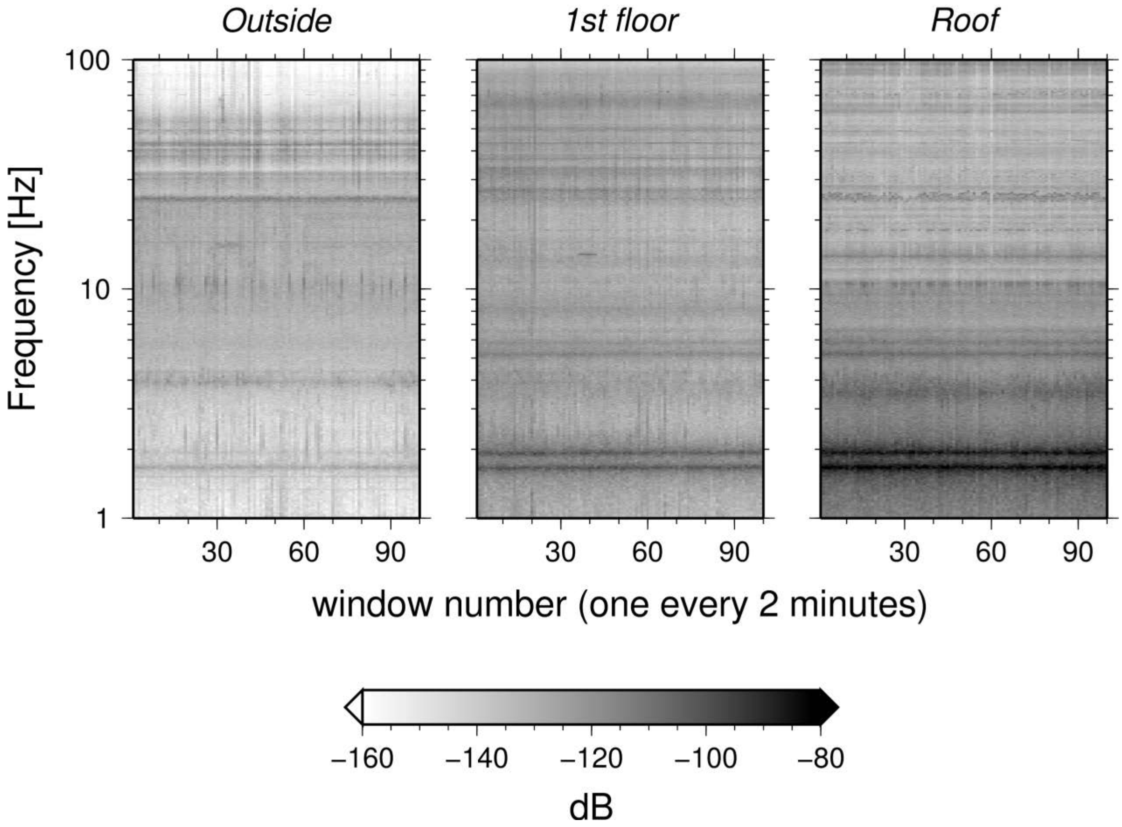

Figure 4: Longitudinal power spectra densities (PSD) computed for the stations installed outside (left panel), on the 1st floor (middle panel) and on the roof (top panel). The spectral values are expressed in decibel (dB) with respect to velocity $[(m/s)^2/Hz]$.

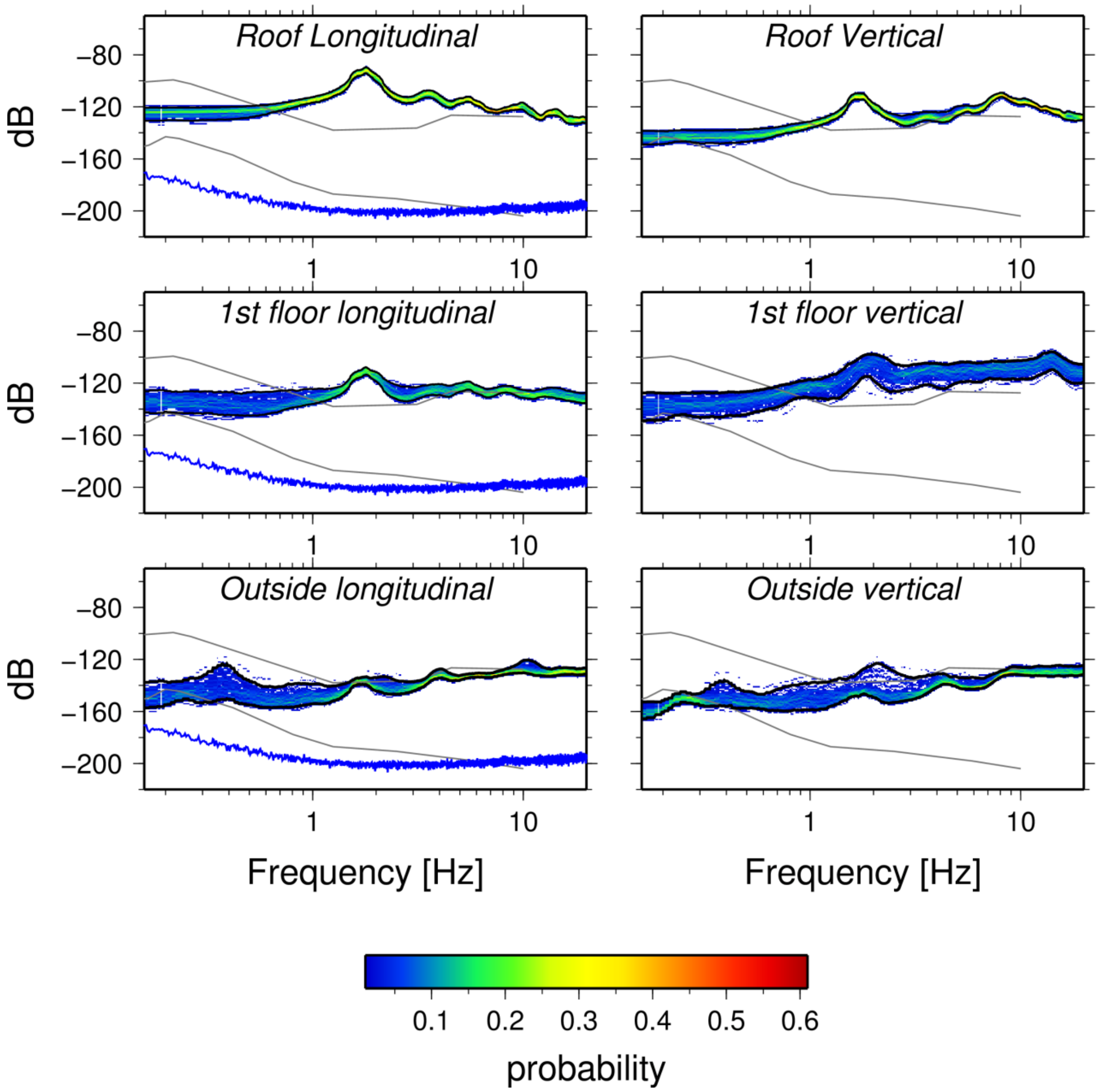

Figure 5: Probability Density Function (PDF) for the stations installed outside the building (bottom), on the first floor (middle) and on the roof (top). The longitudinal components are shown on the left, the vertical ones on the right. The power spectra are expressed in decibel (dB) with respect to velocity [(m/s)^2/Hz]. The black curve identify the 5-th and 95-th percentiles of the distributions. The New High Noise Model and the New Low Noise Model of Peterson (1993) are shown as gray lines. The self noise of the instrument (sensor and digitizer), shown by the blue curve in the longitudinal plots, was derived by coherency measurements (Holcomb, 1989).

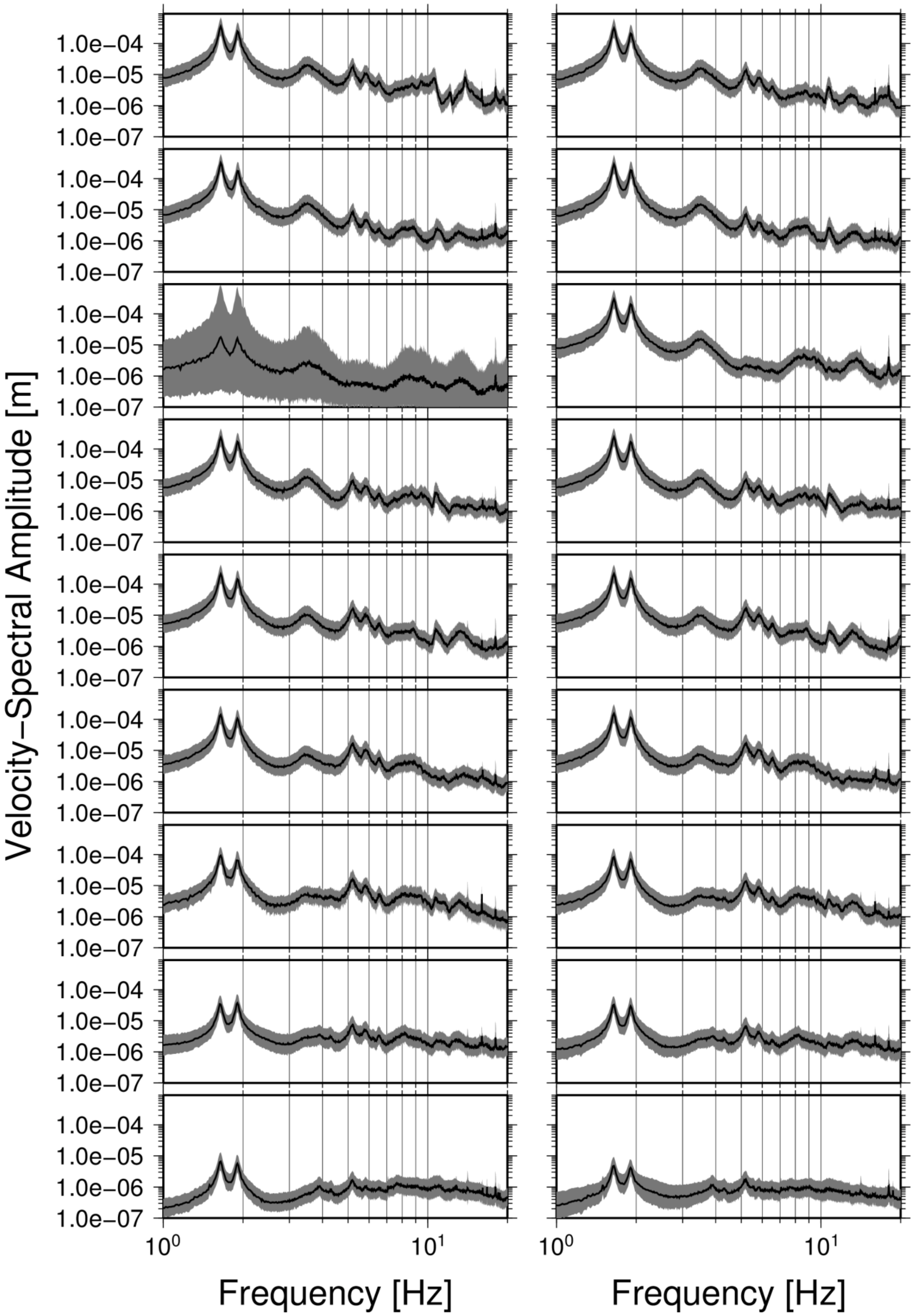

Figure 6: Fourier Amplitude Spectra (FAS) for the longitudinal component, considering the instruments installed along the external (left panels) and internal (right panels) vertical lines of Unit 1 (see Figure 3). The black line indicates the mean value, $\pm 1\sigma$ is shown in gray.

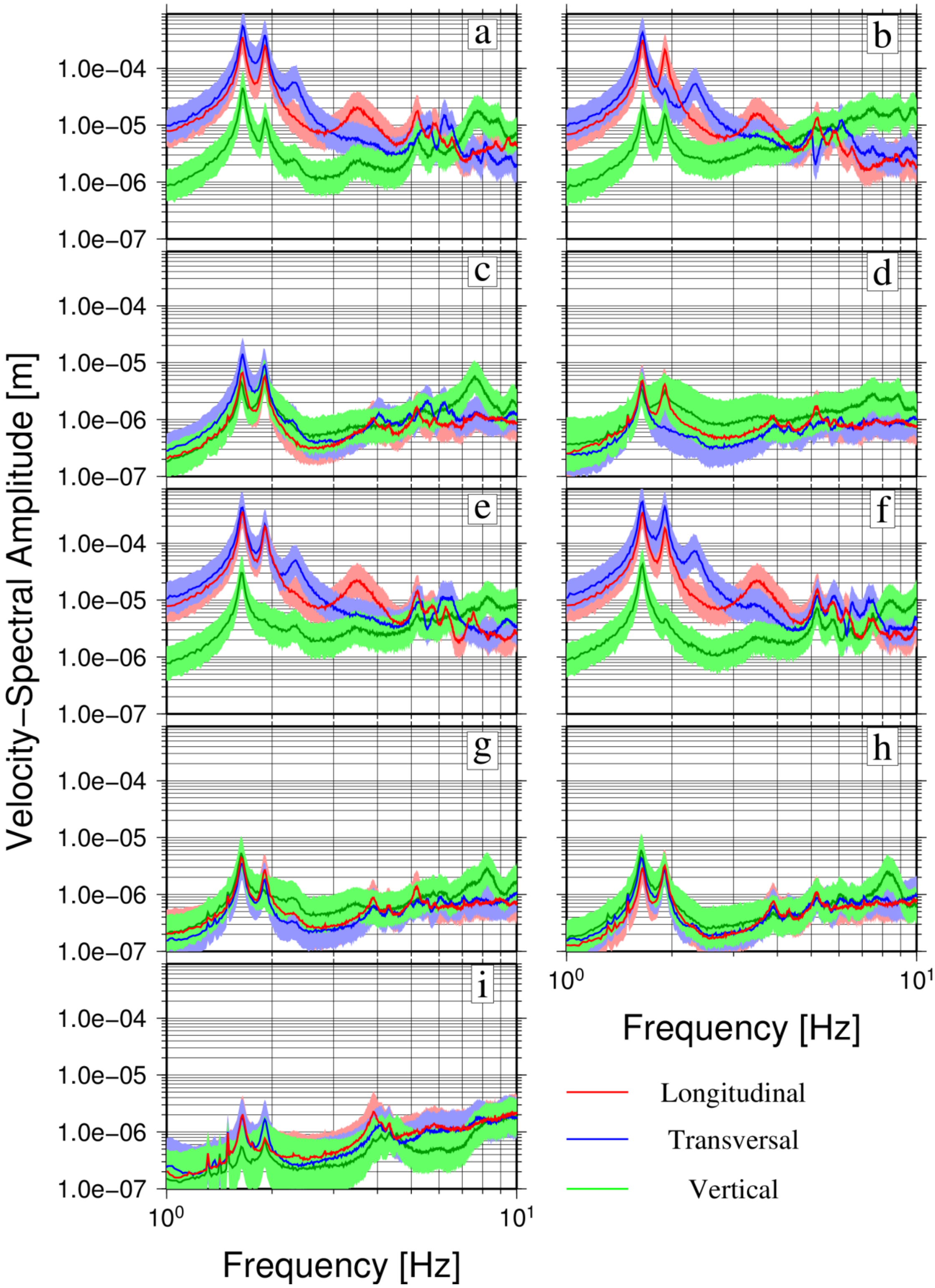

Figure 7: Fourier amplitude spectra (mean ±1σ) for the three components of motion computed for stations installed on the roof (a and b are the two columns in Unit 1; e and f in Unit 2) and in the basement (c and d in Unit 1; g and h in Unit 2). The spectra for the station installed outside AHEPA are shown in panel i.

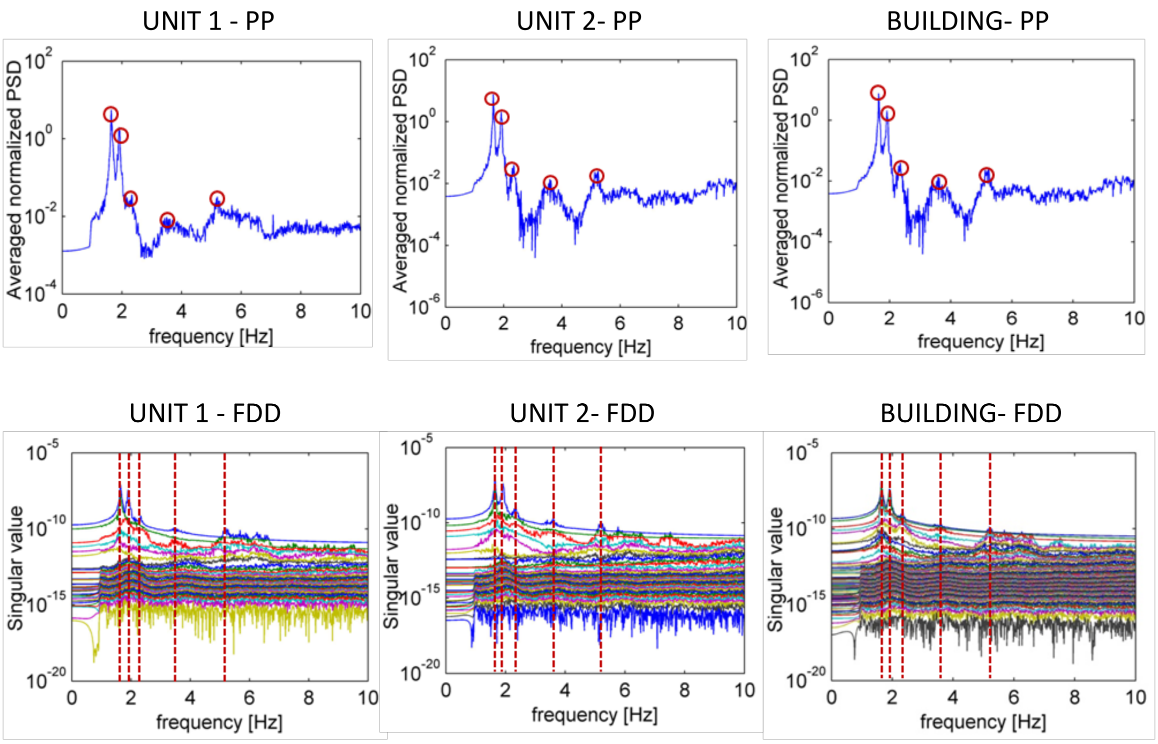

Figure 8: Modal identification using the Peak Picking (top) and the Frequency Domain Decomposition (bottom) applied to ambient noise measurements. The first five modes are indicated with red circles (top panels) and dashed lines (bottom panels).

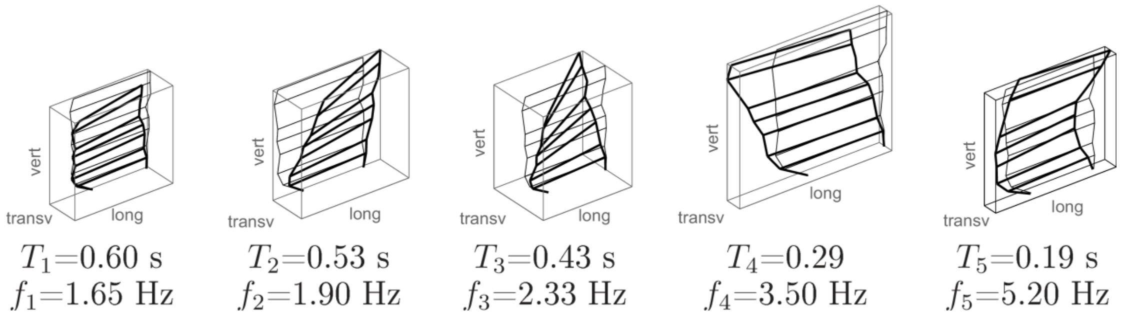

Figure 9: Mode shapes corresponding to the first five identified frequencies for UNIT 1.

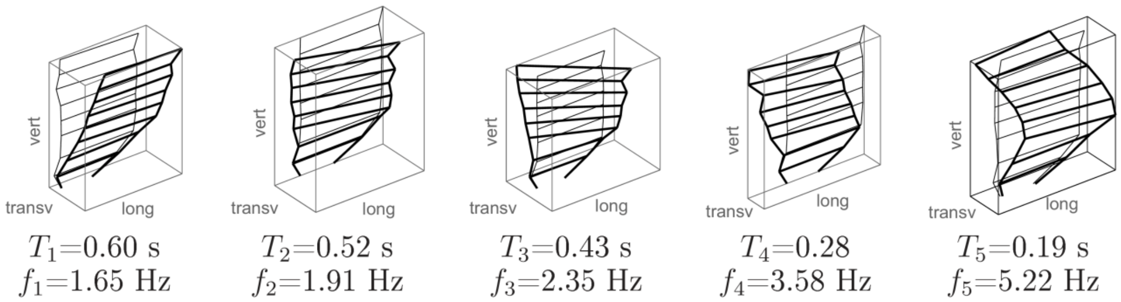

Figure 10: Mode shapes corresponding to the first five identified frequencies for UNIT 2.

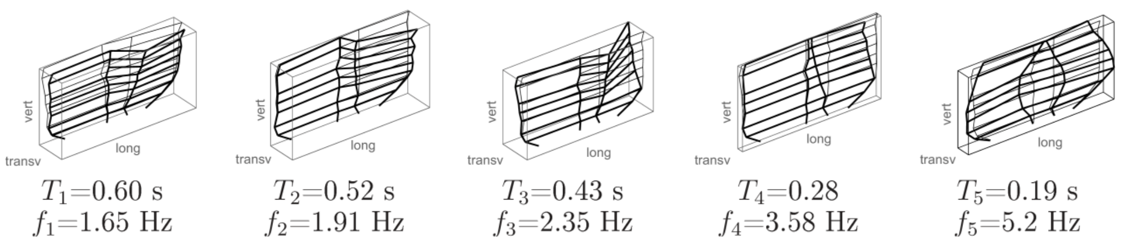

Figure 11: Mode shapes corresponding to the first five identified frequencies for BUILDING.

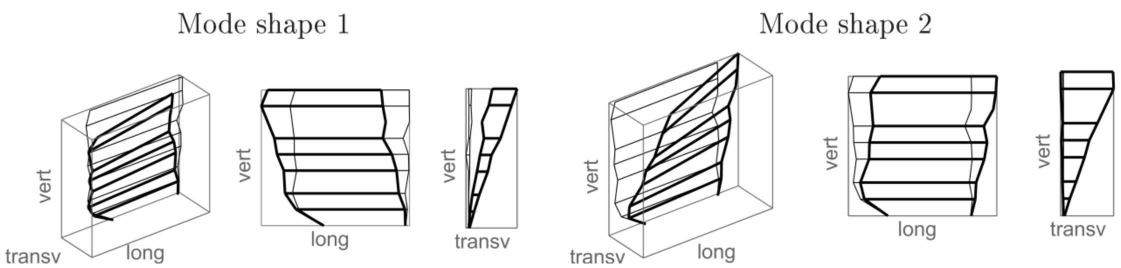

Figure 12: Contribution of the lateral components in the first two modes along the longitudinal and transverse direction for UNIT 1.

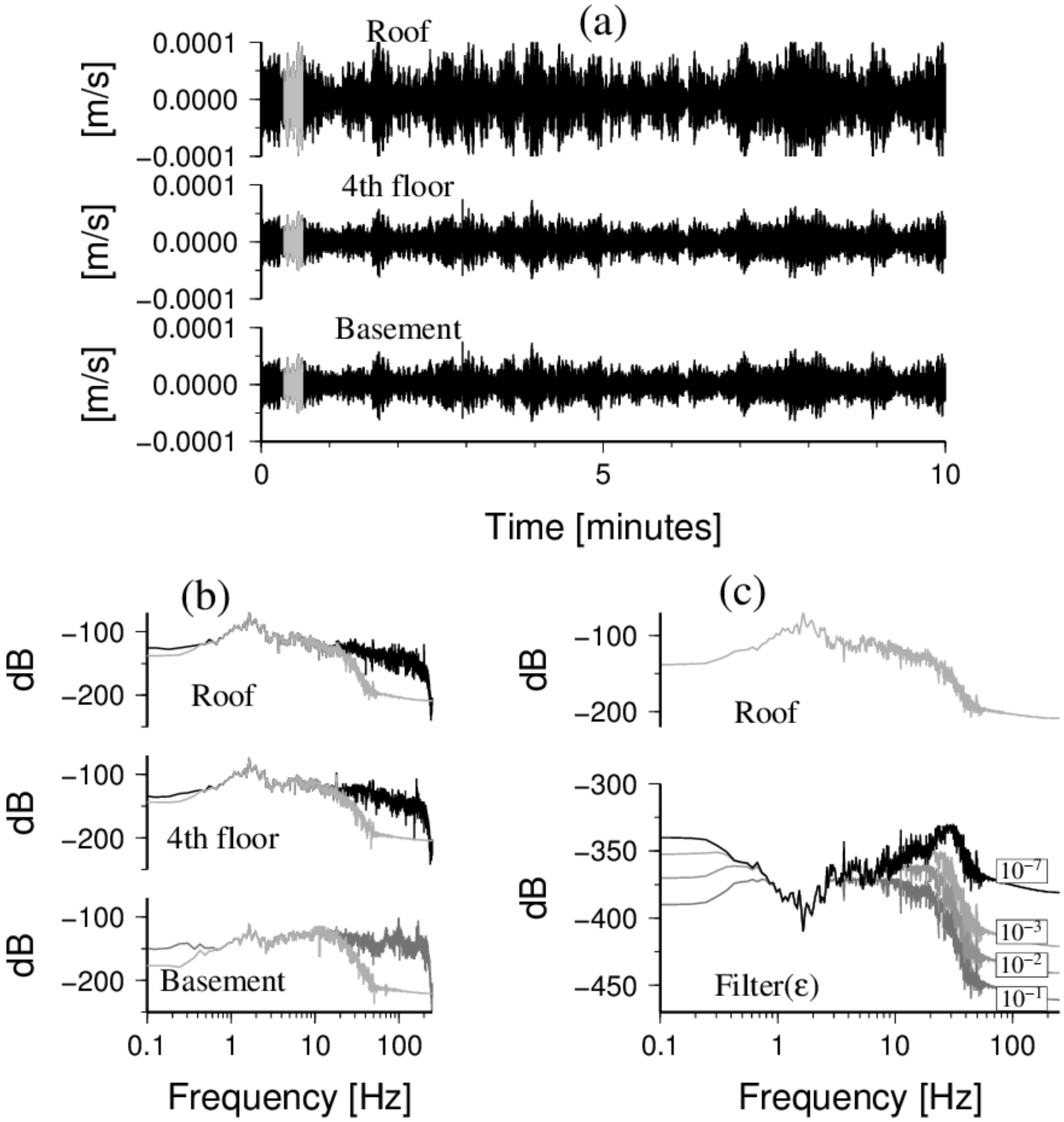

Figure 13: Sketch of the applied deconvolution scheme. (a): velocity recorded at three different locations inside the building; the signal in gray indicates a moving time window used to compute the Fourier spectrum. (b): Fourier amplitude spectra (black) computed for a given time window and filtered spectra (gray). (c): spectrum on roof and filter functions for different values of α (see equation (3)).

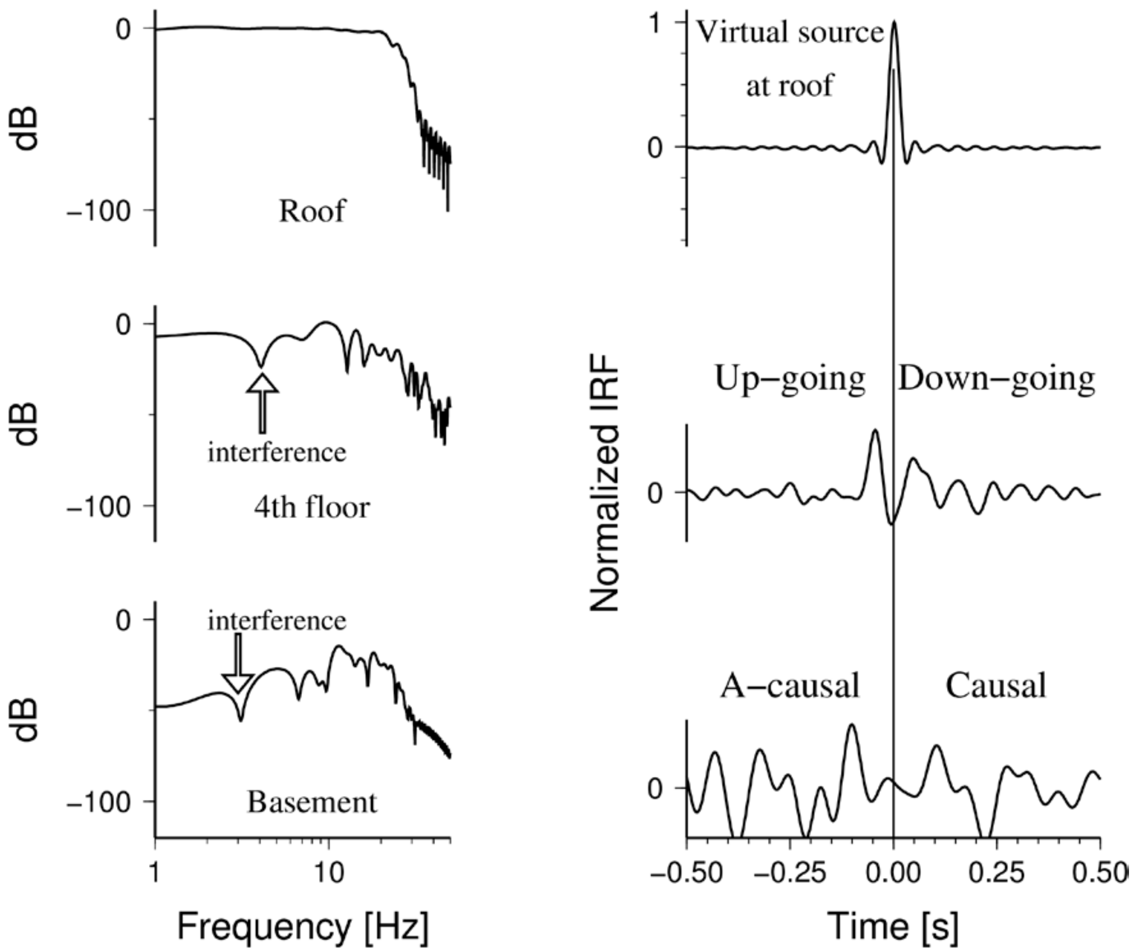

Figure 14: Example of deconvolution results (IRF), computed with respect to the motion on the roof for three different locations within the building. (left) IRFs in frequency domain; (right) IRFs in time domain.

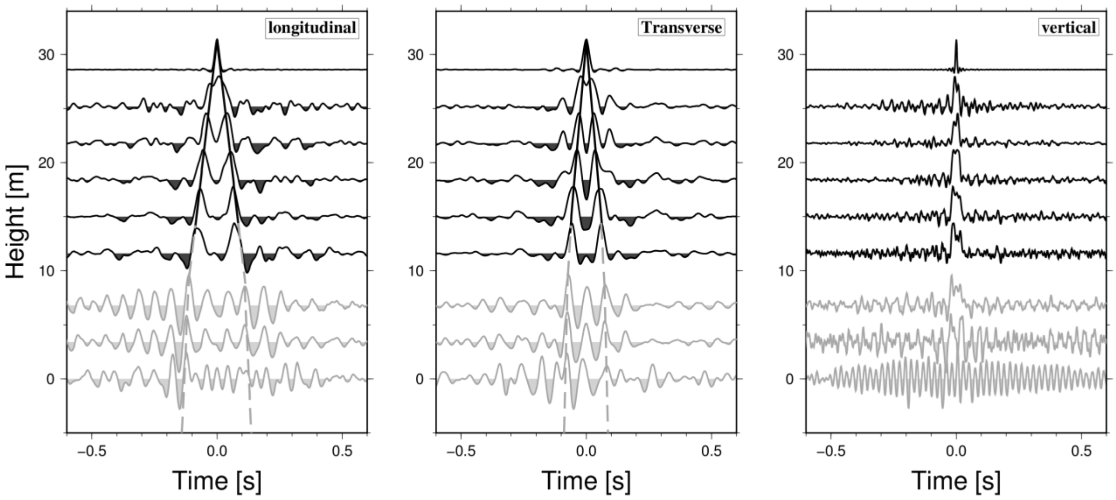

Figure 15: Deconvolution for UNIT 2 with respect to the motion on the roof, considering the three components. The black traces are characterized by the up-going and down-going waves, the gray traces show a more complex pattern. The black lines indicate the average velocities obtained by the interferometry. The dashed gray lines represent the velocities estimated by a comparison of empirical and theoretical IRFs.

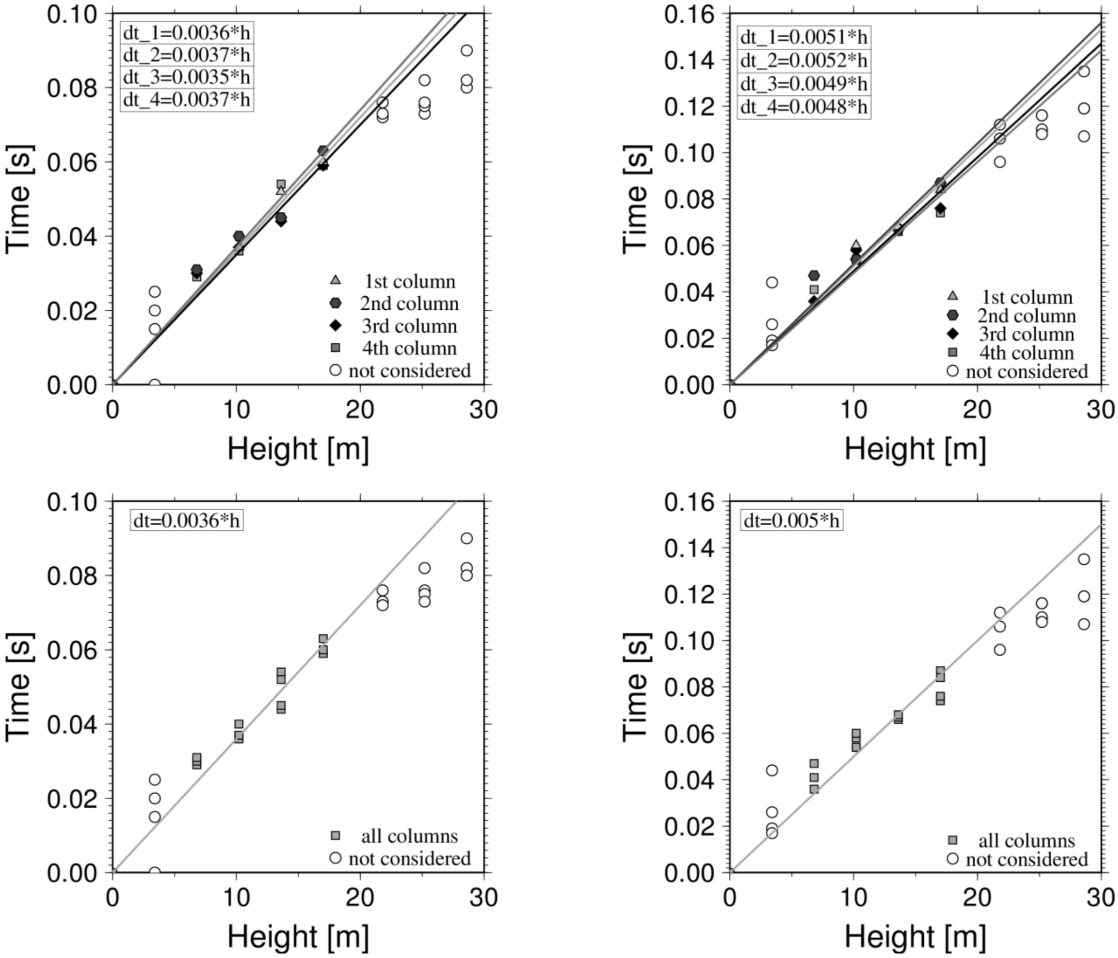

Figure 16: Travel times between the propagation pulses at different floors versus distance to the roof, considering the transverse (left) and longitudinal (right) components. In the uppermost panels, the slowness χ is estimated using a least squares fit, considering the columns separately. Each line indicates the slowness of one column. In the lower panels, the slowness is determined grouping the results of all columns.

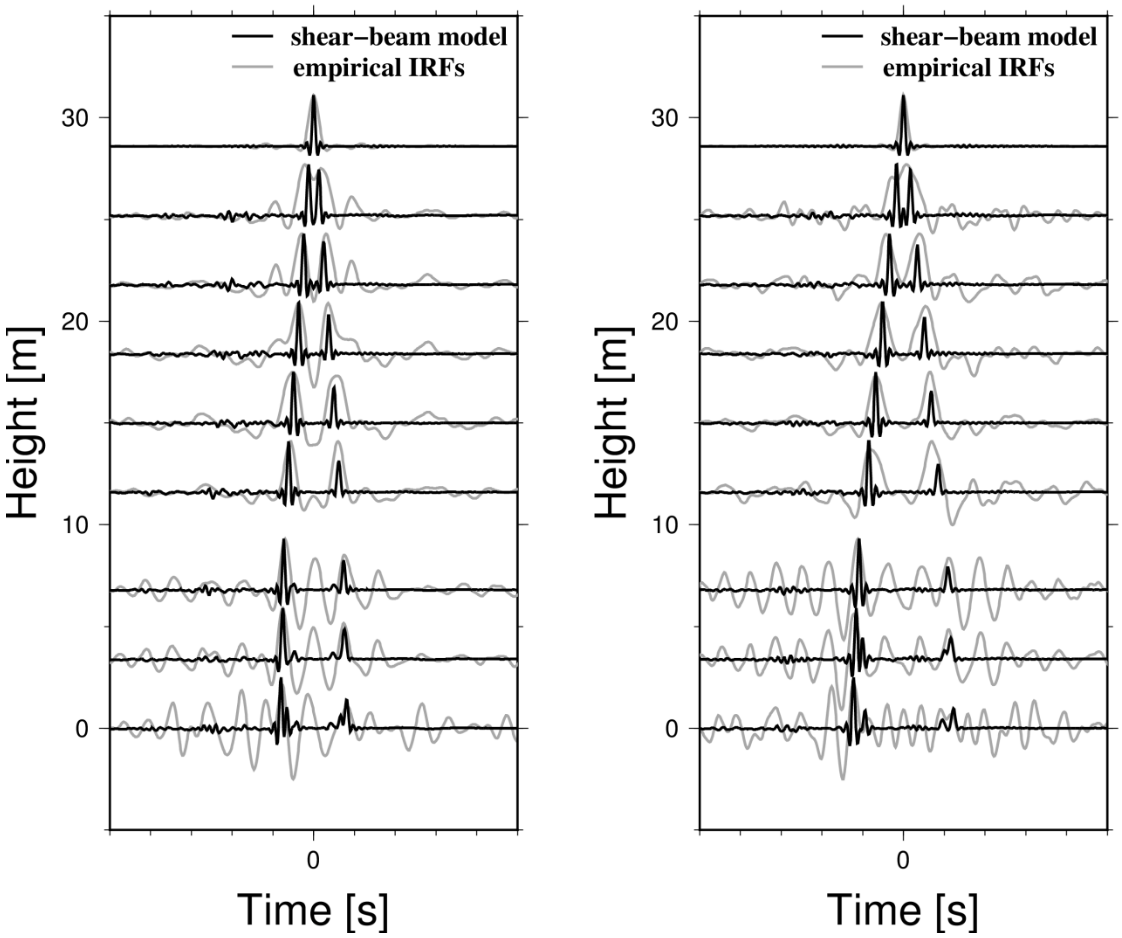

Figure 17: Comparison between empirical IRFs and those computed for the shear-beam model, considering the longitudinal (left) and the transverse (right) directions. For the uppermost floors (3rd floor-roof), the velocities estimated in Figure 16, and listed in Table 3, are used.

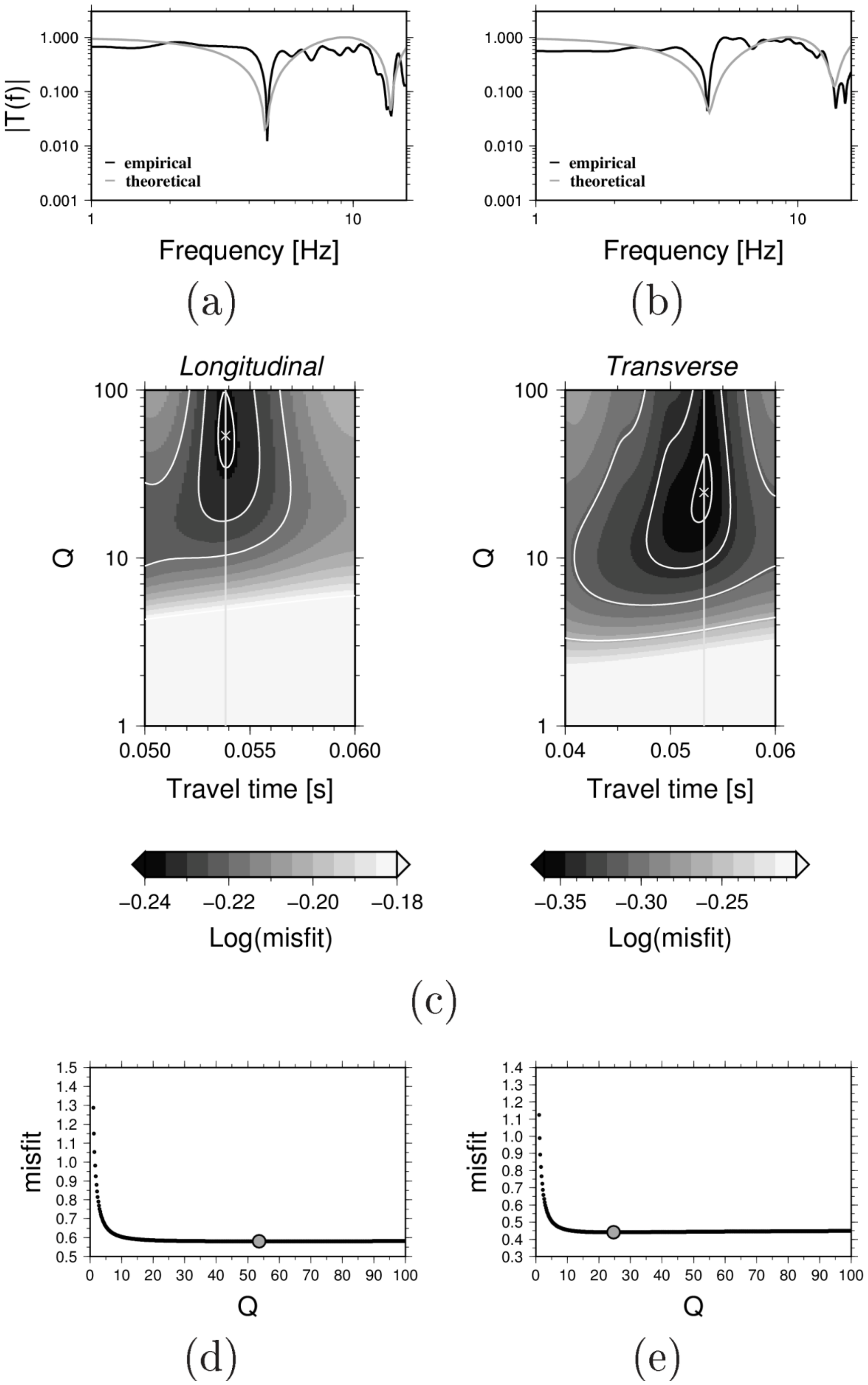

Figure 18: Results for Q estimation using ambient vibration for the longitudinal (left) and transverse (right) directions. (a) Comparison between the empirical (black) and the best fit model IRF spectra (gray); (b) grid search results for different travel time-Q values. The minimum misfit is indicated by a white cross. (c) Cross section along the Q values for the travel time of the minimum misfit function (white line in b). The minimum of Q is indicated by a gray point.

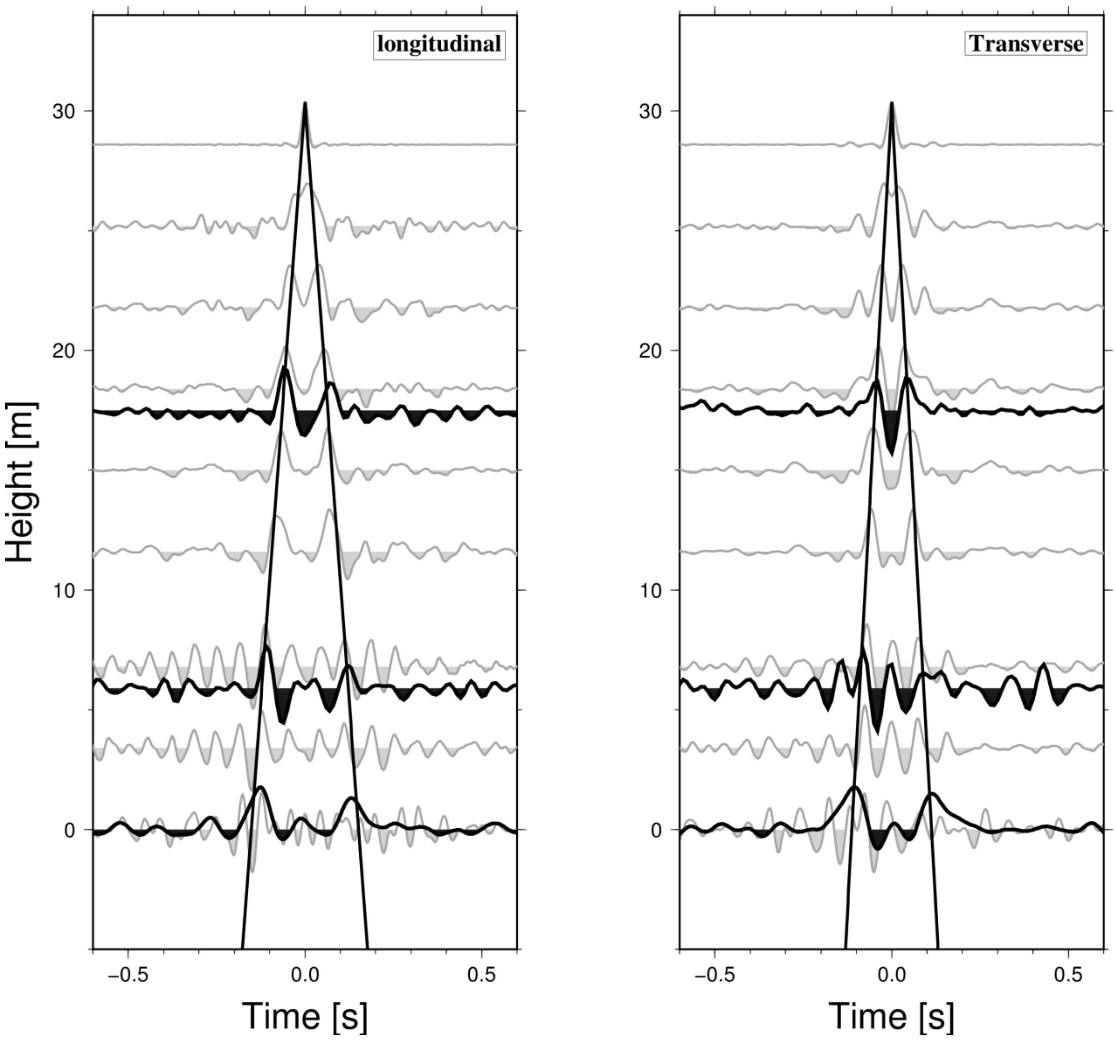

Figure 19: IRFs for noise (gray) and earthquakes (black) for the longitudinal (left) and the transverse component (right). Recordings of two different earthquakes (Volvi earthquake of 11 October 2013; Mw 4.2; distance 38 km and Cephalonia earthquake of 26 January 2014; Mw 6.1; distance 350 km) are used.

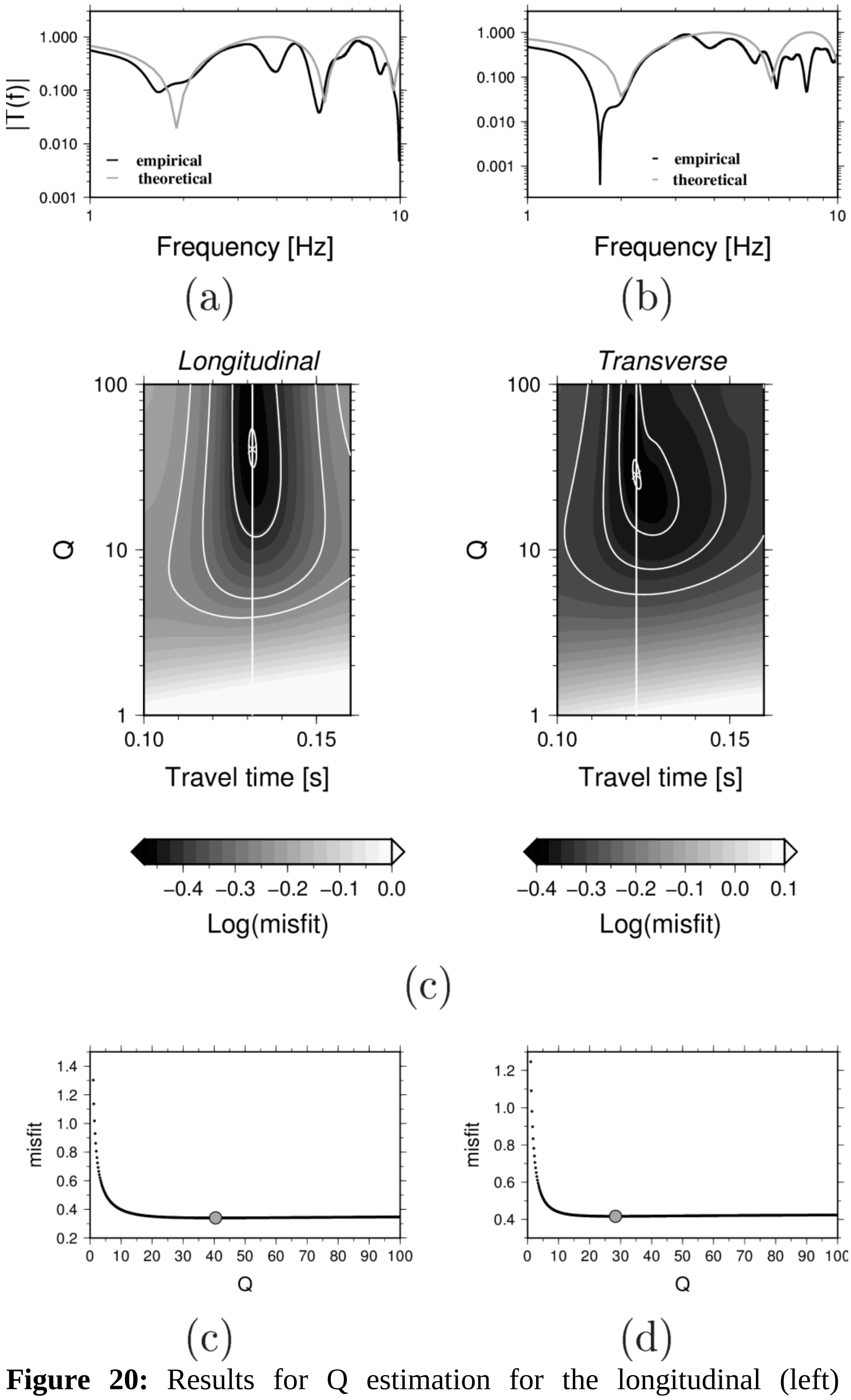

Figure 20: Results for Q estimation for the longitudinal (left) and transverse (right) directions, using a recording of the Cephalonia earthquake. (a) Comparison between the empirical (black) and the best fit model IRF spectra (gray); (b) grid search results for different travel time-Q values. The minimum misfit is indicated by a white cross. (c) Cross section along the Q values for the travel time of the minimum misfit function (white line in b). The minimum of Q is indicated by a gray point.